EXPERIMENTATAL INVESTIGATION OF COMBINED HEAT AND POWER CAPACITIVE DEIONIZATION SYSTEM

A Dissertation
Presented to
The Academic Faculty

by

Jiankai Zhang

In Partial Fulfillment
of the Requirements for the Degree
Master of Science in the
Woodruff School of Mechanical Engineering

Georgia Institute of Technology
May 2017

EXPERIMENTAL INVESTIGATION OF COMBINED HEAT AND POWER CAPACITIVE DEIONIZATION SYSTEM

Approved by:

Dr. Marta C. Hatzell, Advisor
School of Mechanical Engineering
Georgia Institute of Technology

Dr. Matthew McDowell
School of Mechanical Engineering
Georgia Institute of Technology

Dr. Paul A. Kohl
School of Chemical & Biomolecular Engineering
Georgia Institute of Technology

Dr. Shannon Yee
School of Mechanical Engineering
Georgia Institute of Technology

Date Approved: [April 24, 2017]

ACKNOWLEDGEMENTS

Firstly, I would like to express my sincere gratitude toward my advisor, Dr. Marta Hatzell for her guidance and support throughout my master thesis project. She not only provided me sufficient help in terms of research experience but more importantly, she developed my scientific approaches and cultivated my senses of responsibility and professionalism. It is very beneficial and pleasant to work under her guidance, and I genuinely thank for her kindness and patience along the way to complete this thesis. I also appreciate Dr. Kohl, Dr. Yee and Dr. McDowell for being my committee members and providing valuable insights and critiques on my thesis and presentation. In addition, I had the privilege to take Dr. Kohl's electrochemistry and Dr. Yee's heat conduction transfer, which is supportive to the theoretical analysis in this thesis.

I want to give thanks to my lab mates, Mohammadreza Nezami and Daniel Moreno, for their kindhearted help. They assisted me in many aspects of my academic work, including experiments, theoretical modeling, and technical writing. Beyond that, lab cooperation and their encouraging attitudes had a positive influence and motivated me to forge ahead. I am also very thankful to my friends, Xue Xiao, Piyu Sun and Siyao Cai. They lifted up my mood and made my life at Georgia Tech delightful.

Last but not least. I would like to give my most heartfelt appreciation to my parents. It is their unselfish love and encouragement that keeps me motivated to fulfill my objectives of this work.

TABLE OF CONTENTS

ACKNOWLEDGEMENTS iii

LIST OF TABLES vi

LIST OF FIGURES vii

LIST OF SYMBOLS AND ABBREVIATIONS xi

SUMMARY xiv

CHAPTER 1. INTRODUCTION 1

1.1 Global Water Shortage 1
1.2 State-of-The-Art Desalination Technologies 2
1.3 Capacitive Deionization (CDI) 4
1.4 CDI Research Background 6
1.5 Heat-Combined MCDI System 7

CHAPTER 2. LITERATURE SURVEY 10

2.1 CDI Historical Background 10
2.2 CDI Electrode Materials 12
2.2.1 Activated Carbons 14
2.2.2 Carbon Aerogels 14
2.2.3 Ordered Mesoporous Carbons 16
2.2.4 Carbide-derived Carbons 18
2.2.5 Carbon Nanotube
2.3 Capacitive Deionization Performance Criteria 19
2.3.1 Salt Adsorption Capacity 19
2.3.2 Average Salt Adsorption Rate 23
2.3.3 Charge Efficiency 25
2.3.4 Current Efficiency 28
2.4 System architecture 29
2.4.1 Two-Electrode Based CDI Geometries 30
2.4.2 Membrane Based CDI Geometry 33
2.4.3 Flow-Electrode CDI Geometry 34
2.5 Theory of Electrical Double Layer (EDL) 36
2.5.1 EDL Structure 36
2.5.2 EDL Theoretical Models 37
2.5.3 EDL Theories in CDI 39

CHAPTER 3. METHOD 43

3.1 Electrode Fabrication 43
3.2 Experiment Setup 45
3.2.1 CDI and MCDI Cell Assembly 45

3.2.2 System Configuration 46
3.3 Experiment Techniques 50
3.3.1 Cyclic Voltammetry 50
3.3.2 Electrochemical Impedance Spectroscopy 52
3.3.3 Chronoamperometry 54
3.3.4 Chronopotentiometry 56

CHAPTER 4. RESULTS AND DISCUSSION 59

4.1 Theoretical Modelling 59
4.2 Effect of Temperature 64
4.3 Effect of Salt Concentration 72
4.4 Energy Analysis 74

CHAPTER 5. CONCLUSIONS 82

APPENDIX A. MATLAB CODE 84
A.1 MATLAB Code for EDL Potential 84
A.2 MATLAB Code for Charge Efficiency 86

REFERENCES 91

LIST OF TABLES

		Page
Table 1	Quantitative values of resistive and capacitive elements of the MCDI cell. An equivalent electrical circuit is used to simulate the Nyquist diagrams generated by EIS technique. The MCDI cell is operated at 3 different salt concentrations and temperatures.	73
Table 2	The energy analysis under different operating conditions (temperature and salinity) in 3-stroke intermittent cycle (Charging-OCV-Discharge).	81

LIST OF FIGURES

		Page
Figure 1	Schematic of the traditional flow-by CDI cell consists of two oppositely placed porous carbon electrodes and an in-between flow channel. Through imposing an electrical voltage difference, the salt ions in the feed water are forced toward the oppositely charged electrode, developing an EDL at the interface between solid and electrolyte.	5
Figure 2	Schematic demonstrations on MCDI cyclic operation where influent brackish water is separated into freshwater and brine stream through ion adsorption and desorption process. (a) Systemic view of water product and energy flow through ion adsorption-desorption cycles: the electrical energy is consumed to remove ionic species from feed brackish water and partially recovered by cell discharge. Introducing waste thermal energy into the system is suggested to reduce the overall electrical consumption. (b) Change in the salt concentration of brine and freshwater stream at different water recovery ratio with respect to mole of NaCl transferred from freshwater to brine in 1 Liter of influent brackish water. Higher water recovery results in more concentrated brine stream.	9
Figure 3	Schematic descriptions of macropores and micropores as describing the ion transport within carbon electrodes, which differs from IUPAC definitions. (Ref. [1])	13
Figure 4	Maximum salt adsorption capacity (mSAC) values reported for capacitive, composite, hybrid, and flow electrodes in CDI testing from year of 1995 to 2015. (Ref. [2])	22
Figure 5	Kim-Yoon diagram that correlates the average salt adsorption rate (ASAR) and salt adsorption capacity (SAC). The experimental data was acquired as periods of charging (1.1~1.3 V) and discharging (0 V) are the same. Half-cycle time (HTC) is then defined as a half of the value that SAC divided by ASAR. The theoretical calculations are based on EDL and ion transport theory. (Ref. [2])	25
Figure 6	Energy consumption versus charge efficiency for CDI and MCDI based on experimental data. (Ref. [2])	28
Figure 7	Four types of CDI cell geometry (Ref. [1]): (a) Flow-by geometry (b) Flow-through geometry (c) Electrostatic ion pumping (d) Carbon rod electrode wires.	32

Figure 8	Schematics of flow-electrode CDI. The suspended carbon slurry (5-20 wt.% of activated carbon) is used as flowing electrodes for continuous desalination.	35
Figure 9	The components and SEM images of activated carbon electrodes. (a) Three components used to fabricate the carbon film electrodes (activated carbon powder, carbon black, PTFE) and their weighting percentage. (b) SEM images of electrode captured at 2 different resolutions.	44
Figure 10	(a) The CAD design of CDI cell consists two end-plates, two current collectors, two activated carbon electrodes and one silicone rubber gasket. (b) The actual assembly of CDI cell.	46
Figure 11	The calibration curve and fitting equation for converting conductivity values to mass concentration and molar concentration.	48
Figure 12	(a) Schematic view of the overall experiment setup. The CDI or MCDI cell is operated in a batch mode, where the sample solution is pumped from one reservoir to the cell and returns back into the same reservoir. A conductivity probe is submerged into the bulk stream to measure the salt concentration. (b) The actual layout of the overall system in CDI or MCDI experiments	49
Figure 13	Cyclic Voltammetry (CV) diagrams obtained at 3 different flow rate (v = 2, 5, and 10 mV/s), and concentration of salt water in CDI cell is 500 mM.	52
Figure 14	The experimental Nyquist diagram of MCDI cell generated by EIS technique and the corresponding fitting curves simulated based on an equivalent electrical circuit. (c=5 mM and T=21°C)	53
Figure 15	The charging-discharge cycles of MCDI cell operated by CA technique (constant voltage mode). The current response and conductivity changes are demonstrated. Initial concentration of NaCl solution is 5 mM, and the cell was charged and discharged at 1.2 V and -1.2 V.	55
Figure 16	(a) Traditional charging-discharge cycles of MCDI cell operated by the CP technique: The cell is charged at 1.5 mA and discharged at 0 mA, while the initial ion concentration of NaCl solution is 5 mM. (b) The voltage response in a 3-stroke intermittent cycle: an OCV flushing mode is interposed between the charging (3 mA) and discharge (-1.5 mA) steps.	58
Figure 17	Theoretical computation of EDL voltage based on Gouy-Chapman-Stern (GCS) model and Poisson-Boltzmann equation at experimental operating conditions. (a) Temperature dependence of	60

EDL voltages for 3 different salt concentration. (b) The change of EDL voltage with respect to the charge density for different operational conditions

Figure 18 (a) The electrical surface charge density versus cell voltage at different salt concentration. The corresponding theoretical method is based on GCS model. (b) The charge efficiency at different salt concentration and Stern layer capacity is plotted with respect to the cell voltage. 63

Figure 19 The cyclic voltammetry (CV) diagrams of CDI cell at different temperatures (21°C, 35°C, 50°C). (a) The potential sweep rate is 2 mV/s and salt concentration is 5 mM. (b) The potential sweep rate is 10 mV/s and salt concentration is 500 mM. (c) The potential sweep rate is 2 mV/s and salt concentration is 500 mM. 66

Figure 20 The Nyquist diagrams of MCDI cell at different temperature (21°C, 35°C, 50°C) obtained from EIS technique. (a) The salt concentration of NaCl solution is 5 mM. (b) The salt concentration of NaCl solution is 500 mM. 67

Figure 21 The temperature effect on the salt removal of MCDI. The cell is charged and discharged at 1.2 V and -1.2 V for 1 hour at each step, and is operated isothermally at two temperature (21°C and 35°C). 69

Figure 22 Temperature effect on CDI and MCDI cell at various charging voltages. (a) The change of the coulombic efficiency with applied voltage at 21°C and 35°C. (b) The change in salt adsorption capacity with applied voltage at 21°C and 35°C. 71

Figure 23 Nyquist diagram of MCDI cell generated by EIS technique. Three NaCl solution (0.5 mM, 5 mM and 500 mM) is used at room temperature to investigate the effect of salt concentration. 73

Figure 24 (a) 3-stroke MCDI cycle including constant current (3mA) charging with 5mM NaCl, open-circuit (OCV) flush, and reverse-current discharge with different brine concentration. (b) Voltage drop for different concentration of salt water during OCV step. 75

Figure 25 The net electric work represented as the integral of the cell voltage over the surface charge density. At three different salinities (0.5 mM, 5 mM and 500 mM) of the NaCl solution used for open-circuit flushing and discharging the electrode, the overall energy consumptions are calculated as 229.45±4.66 kJ/m^3, 208.71±2.93 kJ/m^3, and 191.23±3.60 kJ/m^3 respectively. 77

Figure 26 (a) 3-stroke MCDI cycle operated using constant-current mode: the cell was charged at 3mA for desalting 5mM NaCl solution, 79

followed by OCV flush and reverse-current discharge with 500 mM brine at different temperatures (21°C, 35°C, 50°C). (b) Voltage drop during OCV at different temperatures.

Figure 27 The overall energy consumption in 3-stroke cycles where the effect of temperature on energy recovery is investigated. 500 mM concentrated brine is used to open-circuit flush and discharge the electrode at three different temperature (21°C, 35°C and 35°C), and the overall energy consumption are calculated as 191.23±3.60 kJ/m^3, 185.41±2.45 kJ/m^3, and 176.55±1.71 kJ/m^3. 81

LIST OF SYMBOLS AND ABBREVIATIONS

σ	Surface electron charge density
c_s	Ion concentration (ionic strength) of the salt solution
k_b	Boltzmann Constant
T	Temperature
N_A	Avogadro's constant
ϵ_0	Electric constant
ϵ_r	Relative dielectric constant
e	Elementary charge
L	Effective thickness of electric double layer
Λ	Charge efficiency
λ	Current efficiency
I	Current
t	Time
c_i	Influent concentration of salt ions
c_o	Outflow concentration of salt ions
V_s	Volume of salt solution
Φ	Flow rate of feed water
V_{dl}	Electrical double layer voltage
V_d	Diffuse layer voltage
V_{st}	Stern layer voltage
V_T	Thermal voltage
λ_B	Bjerrum length
κ	Inverse of Debye length

C_{st}	Stern layer capacitance
R	Lattice spacing
γ	Packing parameter in Lattice gas model
c_s^*	Cross-over surface charge density
δ	Thickness of membranes and silicone rubber gasket
v	Potential sweep rate
i	Instantaneous electric current
m	Electrode mass
V	Cell electrical voltage
ΔV	Voltage sweep window
C_{sp}	Specific gravimetric capacitance
C_{DL}	Double layer capacitance
R_s	Internal solution resistance
R_{CT}	Charge transfer resistance
E_{net}	Net electrical work
E_c	The energy consumption during ion adsorption
E_d	The energy recovery during ion desorption

CDI	Capacitive Deionization
EDL	Electrical Double Layer
MCDI	Membrane based Capacitive Deionization
CV	Cyclic Voltammetry
EIS	Electrochemical Impedance Spectroscopy

RO	Reverse Osmosis
MSF	Multi-stage flash desalination
MED	Multi-effect distillation
ED	Electrodialysis
NF	Nanofiltration
OCV	Open circuit voltage
PTFE	Polytetrafluorethylene
PVDF	Polyvinylidene fluoride
PZC	Potential of zero charge
CNT	Carbon nanotube
PAA	polyacrylic acid
PANI	polyaniline
SAC	Salt adsorption capacity
mSAC	Maximum salt adsorption capacity
eqSAC	Equilibrium salt adsorption capacity
ASAR	Average salt adsorption rate
FCDI	Flow-electrode capacitive deionization
IEM	Ion exchange membrane
CEM	Cation exchange membrane
AEM	Anion exchange membrane
GCS	Gouy-Chapman-Stern model for EDL

SUMMARY

Capacitive Deionization (CDI) is a water treatment technology which removes minority component species through an electrosorption process using porous carbon electrodes. CDI removes salt ions from a bulk mixture through the formation of electrical double layer (EDL). This process is similar to the fundamental mechanism utilized in supercapacitors for energy storage. Once adsorption capacity is reached, the carbon electrodes can release the ions to regain surface area by either short-circuiting or reversing the external voltage. CDI operates in an energy-efficient, cost-effective, and environment-friendly manner, which makes it a promising alternative or supplement to current state-of-the-art brackish water treatment technologies. In recent years, a growing number of researchers have been expanding the CDI field through theory, application and material science. Significant progress has been made in terms of performance, electrode materials, cell architectures, and systematic operation. However, energy recovery and efficiency must be improved in order for CDI to enter the marketplace. Here a combined "heat and water recovery" membrane capacitive deionization (MCDI) system is explored, and new challenges associated with non-isochemical potential brine production during discharge are discussed. This is accomplished through deionizing brackish water in a non-adiabatic cycle. The effect non-adiabatic processes play on whole cycle energy efficiency and salt adsorption is detailed.

In the introduction chapter, I motivate the need for water treatment technologies by discussing emerging trends related to global water stress. After a brief overview of the

state-of-the-art desalination technologies, I highlight the fundamental mechanism and advantages of CDI as a low energy consumption, free chemical contamination and economically feasibility alternative, and summarize the main research topics in CDI filed. Moreover, I highlight the potential of recovering a portion of the free energy (Gibbs) invested in order to perform desalination, and the advances of a heat-combined MCDI system may play in this space.

The next chapter aims to focus on providing a brief perspective on relevant literature, and highlights historical developments and recent findings in the area of CDI. Emphasis is placed on carbon electrode materials and system architectures which significantly affect the level of CDI desalinations. A description of relevant experimental parameters and results are also provided as a reference. Additionally, a review on electrical double layer (EDL) and its applications in CDI support the theoretical modeling performed in this thesis.

Next, experimental and theoretical methodologies are highlighted. Electrode preparation, overall experimental setup, and relevant electrochemical techniques are detailed. CDI cell is constructed using activated carbon electrodes, and a traditional flow-by architecture, and the electrode fabrication and cell assembly are elaborated. The cell is operated in a batch mode cycle and is tested using several electrochemical techniques. On one hand, Cyclic Voltammetry (CV) and Electrochemical Impedance Spectroscopy (EIS) are applied to characterize the cell internal structure and electrode-electrolyte interface.

The ion removal performance of both CDI and MCDI cell are investigated using charge-discharge cycles under constant voltage (Chronoamperometry) and constant current (Chronopotentiometry). The methods for data processing the net electrical work consumed and recovered for a MCDI cell are detailed for both individual cycle processes and entire deionization cycles. The methodology for the dependence of salinity and temperature on energy recovery are also explained.

I next detail relevant experimentally and theoretically obtained results using CDI and MCDI architectures. The theoretical dependence of energy/ion storage within the EDL is evaluated in various temperature and salinities. This analysis provides the foundation for developing new cycles for harvesting waste heat during CDI operations. The contribution of heat addition and brine stream recycle to a MCDI system is then experimentally explored. Within a modified 3-stroke cycle using constant-current method, the influence of varying temperature and salt concentration of brine stream is individually investigated with regard to recoverable energy. The results are discussed and interpreted based on the theoretical modeling and electrochemical characterizations. Key results suggest that increasing the temperature through the addition of heat to a brine stream is beneficial for both higher energy and water recovery. To comprehensively explore the temperature/heat addition effect on brine salinity in CDI and MCDI cells, the electrode capacitance, resistance and cell capacitive elements, are characterized by CV and EIS at different operating temperatures and salt concentrations. Moreover, the influence of increasing temperature on salt removal is further examined by performing conventional charging-discharging cycles at constant-voltage mode. Based on the ex-situ measurements in varying salt

concentrations, desalination performance are evaluated for both CDI and MCDI at experimentally relevant temperatures.

Lastly, I conclude by discussing the practical impact of this work in CDI field, and the potential future work which could aid in further discerning effective deionization cycles and processes.

CHAPTER 1. INTRODUCTION

With increasing stress on global resources (nutrients, metals, minerals, water), the development of technologies which aid in increasing the quantity or quality of these resources are growing in importance. Electrochemical separations based technologies are emerging as a new approach for performing dilute solution separations, and therefore is of interest for many resource recovery and water treatment based processes [2]. Capacitive deionization (CDI), a form of electrochemical separations, is specifically being targeted as an alternative separation technologies for brackish water deionization. Current state of the art ion removal technologies (reverse osmosis, thermal distillation, and electrodialysis) for low saline solutions, have traditionally suffered from many energetic based losses in the 'dilute solution' regimes. CDI by consequence has been shown to achieve high energy efficiency and has the potential for 'built in' energy recovery. The primary aim here is to evaluate CDI from a thermodynamic and experimental perspective, and to evaluate the operational conditions which may improve separations and energy efficiency. Specifically a heat-combined MCDI system which actively harvests waste heat is explored as a medium to improve deionization cycle efficiency.

1.1 Global Water Shortage

Access to freshwater is often seen as a human right. Water is critical for the production of food (agriculture), energy (industry), and is critical in order to maintain most human function. However, with the boost of global population and economic growth, water scarcity has emerged as a serious social, energy and environmental issue [3, 4].

Approximate 1.2 billion of people around the world currently lack access to clean and affordable water [5]. Moreover, many water stress projections forecast that between 2000 and 2025, water withdraws will increase by 25% from 4000 to 5000 km^3, and more than half of the world population daily activities will be affected by water stress [6].

Although water covers 71 percent of earth's surface, fresh water only accounts for 2.5 percent of the total water resources and most of it is either locked in the icecaps and glaciers or found as groundwater. The directly accessible sources of freshwater, like lake and river systems, only represents 0.26 percent of overall water storage [7]. Moreover, the sustainable water supply from Earth ecosystem is estimated to be 4200 billion m^3 each year [6]. Completely relying on existing sources within the natural water cycle will eventually lead to the exhaustion of freshwater resources. To balance the shortfall between supply and increasing demand of freshwater, enormous efforts have taken place to desalinate seawater and brackish water through various types of energy-driven desalination technologies.

1.2 State-of-The-Art Desalination Technologies

Reverse Osmosis (RO), Distillation including Multi Stage Flash (MSF) and Multi Effect Distillation (MED), Electrodialysis (ED) and Nanofiltration (NF) are the commonly known and widely used water desalination methods [8-10]. At present, RO and MSF are the most dominant technologies, representing 59% and 27% of the total global desalination capacity [6].

RO is a pressure-driven process, where a semi-permeable membrane is utilized to separate salt ions and water molecules [9, 11]. The semi-permeable membrane allows for the transport of water molecules but rejects the dissolved ion species, in order to produce freshwater stream. RO is currently used for desalination of both brackish water and seawater. The required salt rejection during brackish water is much smaller than needed during seawater desalination, which ultimately yields water higher flux at lower pressure (~20 bar). Conversely, during seawater desalination, the needs to obstruct the transport of a larger number of ions, creates the need for higher operating pressures (60-80 bar), resulting in larger energy consumption [12]. MSF distillation is a thermally driven process that consists of a series of flashing stages (heat exchangers). The series of exchangers are brought in contact with steam, which causes water to evaporate and separate from the salt [13]. Here, heat recovery process are critical for efficiency, and often the hot brine flows back from the first stage to the last one, where a small amount of vapor is flashed off, since the temperature of brine exceeds its boiling point at the pressure of each stage. The produced vapor further condenses to the distilled water on the outside of the heat-exchanger tubes, meanwhile heating the intake seawater. The flashing process along the stages leads to temperature drop of the unevaporated brine, which corresponds to the decrease in stage pressure.

These two state-of-the-art desalination techniques require a significant amount of energy (mechanical and thermal), since they operate by extracting the major component water from a mixture. The applications of desalination methods among different countries depend on many aspects, including economy, energy resources, and saline water

conditions. In many countries, a large portion of desalination capacities comes from the treatment of brackish water, such as the United States (~77%). The brackish water has a lower salt concentration (below 10 g/L) than seawater (35 g/L), so the energy consumed to remove salt ions in theory is much less than desalinating seawater [14].

1.3 Capacitive Deionization (CDI)

Capacitive Deionization (CDI) is an emerging separation-based technology that has been considered as a potential alternative or supplement to RO for the desalination of brackish waters [1, 2, 14-31]. CDI applies a similar energy storage mechanisms used in electrochemical supercapacitors to remove ions. Specifically, CDI uses of highly porous electrodes with high surface area to remove salt ions from a feed water through an electrosorption process. Traditional CDI cell consists of two oppositely placed porous carbon electrodes separated by a channel for the water flow (Fig 1). CDI operates in a cyclic process, where the brackish feed water is separated into two streams: fresh water and concentrated brine. During the charging (electro-adsorption) phase, an electric potential difference is applied over two porous electrodes. The charged ions in the feed are attracted toward the oppositely charged electrode and immobilized in the pores through the formation of the electric double layer (EDL). The electrosorption of ions results in the reduction of salt concentration of effluent stream, which produces the freshwater desalted stream [1, 2]. Once the charged electrodes approach the adsorption capacity, the discharging (electro-desorption) step can take place by reducing or even reversing the electrical voltage. The salt ions are then released back into the flow channel, resulting in a

highly concentrated waste brine stream. The salt adsorption capacity of carbon electrodes are regenerated during this step. The regeneration processes resemble those used with mixed bed ion exchange resins, however, instead of using expensive chemicals to 'regenerate' ion adsorption capacity, a reverse bias or zero voltage can be applied. The advantage with CDI, is that this 'regeneration' process allows for direct energy recovery, which is not possible with resins.

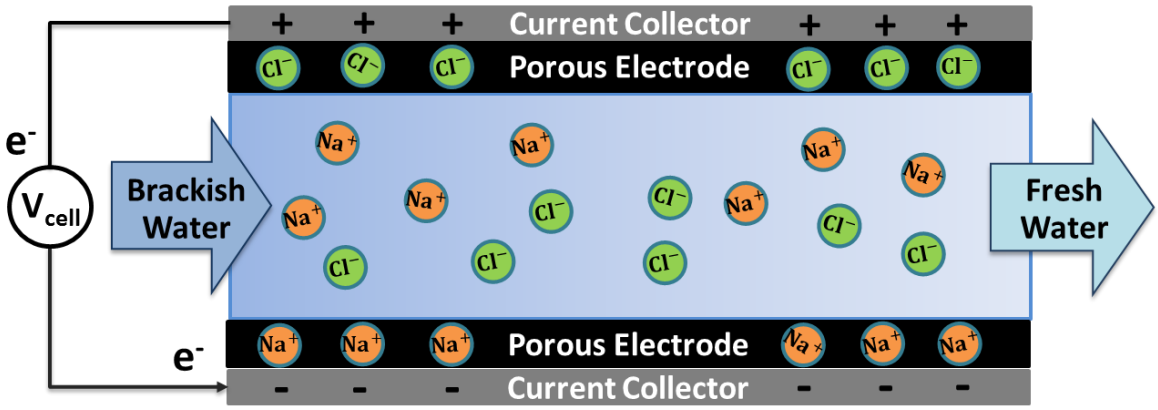

Figure 1: Schematic of the traditional flow-by CDI cell consists of two oppositely placed porous carbon electrodes and an in-between flow channel. Through imposing an electrical voltage difference, the salt ions in the feed water are forced toward the oppositely charged electrode, developing an EDL at the interface between solid and electrolyte.

Unlike most state of the art technologies which separate water (bulk component) from ions (minority component), CDI operates by removing the minority component (NaCl) from the feed water, which diminishes energy consumption. Furthermore, the electrical energy input during the charging step can be partially recovered by discharging the cell. The recoverable energy can be either captured in an ancillary energy storage device or directly used to charge a neighboring CDI cell. Another advantage of CDI, when

compared with polymer based membranes and resins, are the required material are relatively inexpensive, environmentally-friendly, and abundant in nature. The electrodes are typically made from activated carbon, making large scale commercialization feasible.

1.4 CDI Research Background

In the past decade, the number of publications in the CDI area have grown exponentially. Numerous theoretical studies have sought to understand deviations in electrosorption process with complex mixtures (real water) rather than standard electrolytes. This has been accomplished through modeling EDL dynamics to discern changes in ion electrosorption equilibrium process. Experimentally, most efforts have focused on improving cell architecture, electrode materials and operating modes to enhance the desalination performance.

The cell configuration has great impact on the salt removal performance of CDI. Traditionally a flow-by structure has been utilized, yet novel cell architectures such as membrane capacitive deionization (MCDI), flow through electrodes, and flow-electrodes have emerged. MCDI improved the selectivity and energy recovery due to the presences of ion-exchange membranes (IEMs) adjacent to the carbon electrodes. This dramatically boosts the ion adsorption capacity by promoting co-ion exclusion, and counter-ion leakage from the electrodes [32-43]. With IEMs, replacing fixed electrodes with flowing carbon slurry is also possible [44-46]. Flow-electrode CDI provides an avenue for obtaining

‘infinite’ salt adsorption capacity, since it is not limited by traditional film area. This design also enables continuous desalination. Flow through electrodes, where the feed channel is completely removed, allows for the opportunity to minimize ohmic resistance, but this is at the expense of increased pressure requirements and poor contact resistance.

Other key factor that determines salt removal performance is the electrode material, and operating conditions. Various carbon materials have been examined in CDI such as activated carbon, carbon aerogels, carbide-derived carbon, carbon nanotubes, and graphene [1]. Their porous structure were comprehensively characterized in terms of the specific internal area, pore size and intraparticle type. The ion adsorption capacities of those material are further determined in experiments. In terms of operating conditions, several studies have sought to enhance the ion removal and energy efficiency by tuning the charging/discharging voltage or current, frequency, influent salt concentration, and water flow rate [37-39, 47, 48].

1.5 Heat-Combined MCDI System

Waste thermal energy is abundantly available from the industrial exhaust and power plants. Introducing such ‘free’ energy into the MCDI cycles allows for an increase in temperature of saline water (Fig.2a). Since the EDL voltage is not only dependent on applied electrical voltage and influent ionic strength, but increases with temperature, the waste heat acted upon the system can induce a thermal voltage rise across an EDL, which

I propose can be used to negate electrical energy demand. The theoretical calculations based on the EDL modeling and thermodynamics indicates that about 1.42% of the waste heat can be converted to the electrical work stored in the double layer. To determine the influences of raising operational temperatures on MCDI energy recovery, a novel 3-stroke cycle is applied in experiment, where an open-circuit voltage (OCV) mode is interposed between the charging and discharging steps. The temperature of salt solution is tuned within such cycle, and resulting variance in electrical work shows that increasing temperature gains more recoverable energy.

I also aim to evaluate the energetics associated with discharging in a brine stream. Throughout ion adsorption and desorption process, the influent brackish water is separated into freshwater and brine stream. The level of water recovery ratio represents the volumetric percentage of freshwater stream separated from the bulk brackish water. The treatment of 1 liter of the brackish water reservoir with initial 25mM ionic strength, for instance, was expected to reach 1mM of deionized water using MCDI (Fig.2b). Higher water recovery requires more NaCl molecules transferred from fresh water to brine stream, which results in small volumetric but highly concentrated brine solution. In this case, 95% water recovery produces near 0.5 M NaCl solution. In this study, different salt concentrations of brine are used for flushing and discharging MCDI cell in the 3-stroke cycle. The experiment results reveal that recycling the concentrated brine for higher water recovery is advantageous for reduced electrical work throughout operation cycle as well.

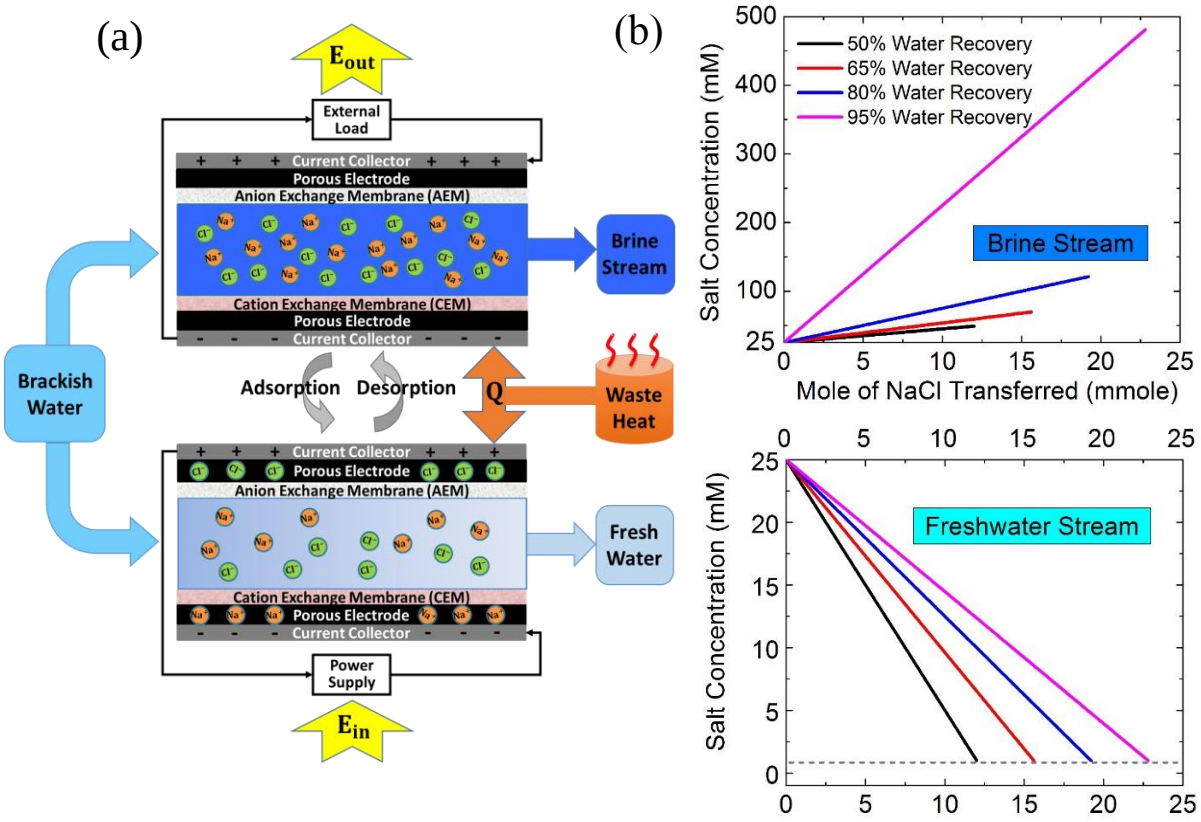

Figure 2: Schematic demonstrations on MCDI cyclic operation where influent brackish water is separated into freshwater and brine stream through ion adsorption and desorption process. (a) Systemic view of water product and energy flow through ion adsorption-desorption cycles: the electrical energy is consumed to remove ionic species from feed brackish water and partially recovered by cell discharge. Introducing waste thermal energy into the system is suggested to reduce the overall electrical consumption. (b) Change in the salt concentration of brine and freshwater stream at different water recovery ratio with respect to mole of NaCl transferred from freshwater to brine in 1 Liter of influent brackish water. Higher water recovery results in more concentrated brine stream.

CHAPTER 2. LITERATURE SURVEY

2.1 CDI Historical Background

CDI originated as a "electrochemical demineralization" and was developed by Blair and Murphy in the early 1960s [49]. This initially observed ion removal processes under an electric field, and however misinterpreted this observation as a Faradaic reaction. Blair and Murphy further claimed that the chemical functional groups aided in securing cations on the carbon surface through an ionic bond [49]. Later it was proposed that demineralization was linked to local electrode pH rather than surface functional groups [50]. These works specifically highlighted the role parasitic electrochemical reactions at the anion and cation responsive electrodes have in shifting the local environmental of electrodes to either an acidic or basic pH. The change in local pH leads to the ionization of weak acidic and basic functional groups at the electrode surface, which could result in ion removal at near neutral conditions. Others even developed a mathematical framework to describe the salt concentration distribution during these proposed processes within a electrochemical demineralization technology [51]. Most of these modeling efforts, neglect the complicated geometry of carbonaceous material, derive understanding of charge carrier dynamics by combining mass balances and transport equations, to discern relationships between ion concentration and time and ion concentration and spatial coordinates. These models can be evaluated under various operation conditions.

Those initial investigations set an important foundation to elucidate the demineralization process. However, many of the proposed hypothesis were later disproven.

An important breakthrough on this topic was made by in 1970 [52], when faradaic reactions on carbon materials were shown to have limited influence on the observed ion removal performance. The theory of "potential-modulated ion sorption" was then evolved, and pointed to the formation of electrical double layer (EDL) as the true mechanism for electrochemical demineralization (ion removal). Furthermore, it was shown that anion and carbon electrodes were not selective to either anions or cations, and could entrap either charged species. These pivotal findings were observed through half-cycle operation conditions, where variable time steps and cell voltages were applied. Johnson and Newman then outlined that the adsorption capacity was dependent on the double layer capacity, electrode internal areas and applied electrical voltage [53].

Since the EDL governs the ion adsorption/removal process, significant modern works related to CDI have focused on explaining and monitoring ion electrosorption process in porous carbon electrodes. Soffer and Folman examined the double layer in high-surface porous electrode through determining the salt adsorption and electrocapillary maximum [54]. The difference in capacity between porous carbon and mercury was observed to be small, suggesting that micropores of smallest size can be wetted and supportive for ion sorption. The ion adsorption was experimentally measured from change in salt concentration and was calculated thermodynamically, and the results were matched within a certain range of potential. Later work by Oren and Soffer proposed a concept of four-action electrochemical parametric pumping cycles, where ion adsorption and desorption are illustrated based on EDL in porous carbon electrodes [55, 56]. The system

configuration, practical operations and evaluating methods introduced in this concept importantly affect the following research and commercialization of CDI.

2.2 CDI Electrode Materials

In addition to mechanisms, significant work has focused on exploring carbon materials. The early work by Murphy and co-workers exploited many conductive and high-surface carbon materials for desalting brackish water [50, 57, 58]. The selections of materials for CDI however, has significantly since these early works and depends on many factors. Carbon is favorable for ion electrosorption due to the highly porous structure. The pore size, pore volume and pore connectivity all have direct impact on the ion transport and ion storage capacity. Ideal ion adsorption requires a large specific surface area to improve salt ions are accessible to a surface [1]. The International Union of Pure and Applied Chemistry (IUPAC) has classified the pores to macropores, mesopores and micropores according to their size. The size of macropores are greater than 50 nm, and that of micropores are smaller than 2 nm. The mesopores are defined when the pore size is in between them [59]. Since most carbon materials exhibit a wide range of pore size, it is less meaningful to characterize them strictly using the average size values. It is also important to note that the terminology of micropores and macropores can be also used to discern the pore shape without the restriction of ion size [28, 60, 61]. Macropores are sometimes referred to the interparticle channels that allow salt ions to transport between smaller pores and the bulk solution. In this context, the micropores means the narrow pores inside of the particles (intraparticle) where ions are strictly held in the EDL (Figure 3). Besides of the

pore structure, the performance of carbon electrodes is also dependent on electrical conductivity, chemical stability, availability of the material, difficulty of tuning the porosity, cost, and lifetime [30]. Next, five carbon based electrodes in common CDI studies are reviewed.

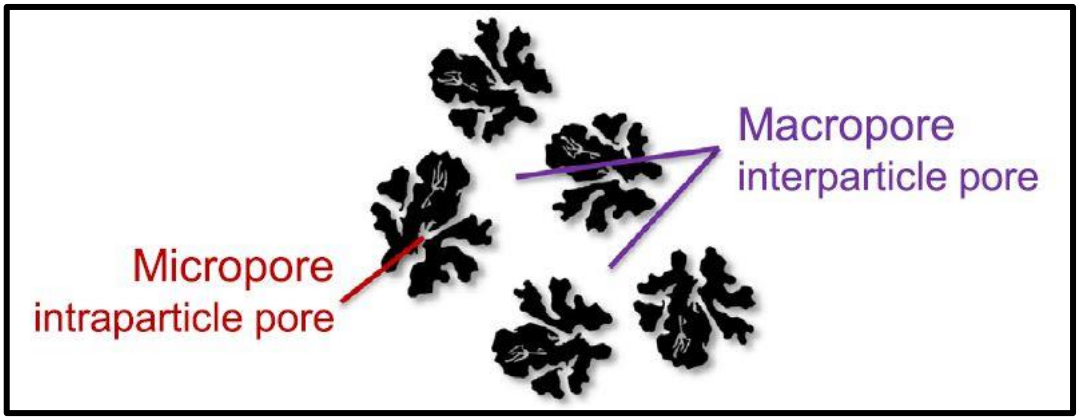

Figure 3: Schematic descriptions of macropores and micropores as describing the ion transport within carbon electrodes, which differs from IUPAC definitions. (Ref. [1])

2.2.1 Activated Carbons

Because of extremely high specific area (1000-3500 m^2/g) and low price (~0.5 €/kg), activated carbon is one of the most prevalent carbon material that has been widely commercialized. Activated carbon is derived from various natural sources (coal, wood, starch, etc.), primarily processed to form a powder with micrometer scale features. The activated carbon powders can then be made into a thin film, and is the primary electrode type used in CDI cells. Films are produced by mixing the activated carbon powder with a polymer binder such as Polytetrafluorethylene (PTFE) and Polyvinylidene fluoride (PVDF), and a conductive material (carbon black). The pore structure of the film electrode

can be affected by precursor materials and synthesis conditions. Since porous structure greatly influence the electrode desalination capacity, it is important to optimize the fabrication procedures to achieve higher ratio of pore volume and specific surface area [1].

Chemical treatment and various synthesis protocols of activated carbons have been employed as a means for enhancing salt adsorption capacity. Many of which have been adopted from carbon based processing for supercapacitors. Activated carbon chemically treated with KOH has been shown to increase the hydrophilic (wetting) nature of the surface changed which improves performance, through increasing the active accessible area [16]. Higher charge efficiency has been achieved through both reducing or oxidizing the activated carbon fibers [62]. Activated carbon fibers oxidized in a concentrated nitric acid (HNO_3) solution, drives the potential of zero charge (PZC) in a positive direction, which reduces the desired whole cell potential needed to adsorb ions. Reduction oxidized surfaces, using gas phase hydrogen reaction at high temperature (~1000°C), and $NaBH_4$ resulted in a negative shift in PZC which was not stable. A three-electrode asymmetrical cell was applied to maintain the electrode surface treatment, causing a higher charge efficiency and desalination capacity. Others explained that these treatment processes may enhance salt removal due to independent ancillary Faradaic like reaction [63].

2.2.2 Carbon Aerogels

Carbon aerogels attracts attention in CDI application because of its high electrical conductivity (25-100 S/cm), low resistivity (400 Ω·m/cm), and middle range of specific surface area (400-1100 m^2/g) [1]. The first study of carbon aerogels in CDI application is conducted by Farmer et al. [64] They reported the specific surface area of carbon aerogels (400-1100 m^2/g) and proposed several important applications of CDI with this material. The aqueous solutions of NaCl and $NaNO_3$ are used as feed stream to examine the desalination performance at carbon aerogels at different applied voltage. They also performed aging studies on electrodes, and found the electrosorption capacity decreases 6 to 8 percent after months of operation at 1.2 volts, but reversing the electric potential periodically mitigate the rate of capacity loss [65]. Another study from Farmer et al. emphasized on electrosorption of trivalent and hexavalent chromium species from untreated ground water by using carbon aerogels [66]. The ionic species in the feed species exhibit as Cr(III) and Cr(VI), and the concentration of chromium in effluent water was observed after hours of operation. Gabelich et al. utilized carbon aerogels in CDI cell to desalinate both laboratory and river waters containing multiple ionic species (Ca^{2+}, Mg^{2+}, K^+, Na^+, SO_4^{2+}, NO_3^-, Br^-, Cl^-, etc.) [67]. The adsorption capacity of carbon aerogels was determined from 1.0×10^{-4} to 2.0×10^{-4} equivalent per gram of electrode. Gabelich et al. claimed that the selectivity of ion electrosorption was dependent on the ionic hydrated radii. The monovalent ions with smaller hydrated radii have greater tendency to be adsorbed over multivalent ionic species, and the electrosorption of organic species with large hydrated radii is damaging to the pore structure of the carbon aerogels. Yang et al. tested a carbon aerogel composite with silica gel which exhibited a larger specific surface area (900-1700 m^2/g) [68].

2.2.3 Ordered Mesoporous Carbons

The ordered mesoporous carbon differs from activated carbon electrode, because it has highly ordered pore structure that displays a periodic arrangement such as cubic or hexagonal shape [69]. To fabricate ordered mesoporous carbon electrode, a template is required to format the carbon particles in a nanomater scale. There are two templating methods (hard and soft templating) that shares similar principle: the carbon precursor is shaped within the template, which followed by template removal either chemically or physically [1, 63]. The specific surface area of ordered mesoporous electrode is comparable with that of activated carbon, and is generally in the range from 750 to 1500 m^2/g. The ordered structure is favourable for the ion transport inside of the electrodes, resulting an enhanced electrosorption capacity. However, higher manufacturing cost makes it difficult for large-scale commercialization.

Li et al. synthesized two types of ordered mesoporous carbon electrode via a modified sol-gel process and examined their pore structure and desalination capacity [70]. It was found that generating crown-ether type complexes between triblock copolymers and nickel ions leads to higher surface area and smaller pore size. Introducing $NiSO_4 \cdot H_2O$ into the ordered mesopores electrodes further improves the pore structure, where the pore size is 3.7 nm and specific surface area is 1491 m^2/g. Moreover, higher ion adsorption capacity is obtained compared to other ordered mesoporous carbon and activated carbon electrodes. Consistent trend is shown in another study [16]. The order mesopores electrodes with smaller specific surface area yielded greater electrosorption performance as compared to

the commercial activated carbon electrodes with even higher surface area. This implies highly ordered mesopores contribute to larger effective surface area for electrosorption of salt ions. In addition, Wen et al. combined the hard and soft templating method to synthesize a three-dimensional hierarchical porous carbon [71]. Such electrodes shows superior electrosorption capacity and regeneration performance over the normal ordered mesoporous carbon electrodes.

2.2.4 Carbide-derived Carbons

Carbide-derived carbon recently draws attention due to the precisely tailored pore size distribution. Unlike the ordered mesopores carbon, it does not have periodic pore arrangement, but it features in extremely narrow micropores with small variance in pore size. Carbide-derived carbon are commonly synthesized by impregnating the carbide powders in dry chlorine gas at high temperature (200-1000°C) and then conducting hydrogen annealing to removal residuals of chlorine compounds. This specific surface area of this material generally ranges from 1200 to 2000 m^2/g, but can reach uttermost level of 3200 m^2/g. Porada et al. experimentally investigated the effect of pore structure on electrosorption capacity and salt removal rate by using carbide-derived carbons and ordered mesopores silicon carbide-derived carbon, whose pore sizes are 1 and 4 nm [72]. Two material shows similar but extremely high values of ion adsorption capacity, which unit gram of electrode removes 15 mg NaCl. They also correlated the desalination performance with pore size increment quantitatively, and demonstrated the ion electrosorption behavior can be directly predicted by analysing pore size distributions.

However, some other studies claimed that mesopores with size of 3-4 nm is optimum for ion removal in CDI, considering micropores may restrict the dynamic ion transport and induce the overlapping of EDL [16, 70, 73].

2.2.5 Carbon Nanotube

Carbon nanotube (CNT) is a versatile nanomaterials since its discovery in 1991 [74]. The small specific surface area is non-ideal for CDI, yet the tube-shaped structure could promote ions transport. Some recent studies have examined CNT as a potential porous electrode in CDI, but the metal catalysts presented in CNT may invoke side reactions during the desalination process, which contaminates produced water stream and degrades the electrode. Another disadvantage appears due to the high cost of material compared to the conventional activated carbon electrodes.

Others have synthesized a multi-wall CNT from binary aerogels catalysts through methane chemical vapor decomposition at high temperature (~680°C) [75]. The produced electrode was analysed via transmission electron microscopy, X-ray diffraction and Raman spectroscopy, and its capacity of desalination was also determined. The surface area was found between 50 to 129 m^2/g. They also modified the surface of CNT electrode by ultrasonic in HNO_3 solution and ball milling, which shown a greater salt removal performance. Multi-wall CNT electrode was also explored in a CDI cell, and showed similar range of specific area (47-129 m^2/g) [31]. To compare the CNT with activated

carbon in terms of desalination, the composite electrodes made up of activated carbon and CNT with different ratio were prepared. Smaller adsorption capacity of electrode was observed at higher ratio of multi-wall CNT constituent. On the contrary, Zou et al. reported that the electrosorption capacity of CNT with lower specific surface area is greater than that of activated electrode with larger surface area [76]. The comparison was also made between the single-wall CNT with multi-wall CNT, and showed the former one is superior in salt removal [77, 78].

2.3 Capacitive Deionization Performance Criteria

Standardization and benchmarking practices have emerged as an important practice to predict the actual performance of commercial grade CDI cells. Most criteria focus on understanding desalination performance though salt adsorption capacity, salt removal rate and salt removal efficiency and the energetics associated with desalination using charge efficiency and current efficiency measures. Here, progress and targets associated with each performance criteria are highlighted.

2.3.1 Salt Adsorption Capacity

The salt adsorption capacity (SAC) is the most common parameter to evaluate salt removal in CDI testing. It is defined as the mass of salt ions adsorbed per unit of the representative electrodes. SAC values are commonly gravimetrically (mg/g) or volumetrically (mg/mL). The gravimetric SAC is widely used in literature, with the

electrode mass referring to the mass of the entire electrode (carbon, binder, additives, etc.) in dry conditions [72, 79]. While volumetric SAC sometimes provides pertinent information which aids in understanding potential system size, gravimetric approaches are much more important for evaluating research progress. In a single pass mode where the effluent salinity is measured at the exit of the cell, and the SAC is calculated as shown in Equation 1.

$$SAC_{single-pass} = \frac{\Phi \cdot \int [c_i - c_o(t)]\, dt}{m} \quad (1)$$

where m is the total electrode mass, Φ is the flow rate of feed water, c_i and c_o represent the salt concentration of influent and effluent stream. Therefore, the time integral of change in salt concentration multiplied by the flow rate lead to the amount of salt adsorption in mass. Under a batch mode, the effluent stream is recycled through the cell, and salt removal is obtained by directly multiplying the change in salt concentration with total volume of salt solution V_s [1, 2]. The calculation of SAC for batch mode is shown in Equation 2.

$$SAC_{batch} = \frac{(c_i - c_o) \cdot V_s}{m} \quad (2)$$

While charging CDI cell by an applied voltage, the electrodes can reach the maximum or equilibrium adsorption capacity (mSAC or eqSAC) after a long duration. At a constant charging voltage, the equilibrium state is obtained when the amount of electron charge on electrode surface remains unchanged. By that time, no additional ion adsorption occurs and salt concentration of effluent stream keeps constant, which is reflected by same measurement in conductivity of water. It is important to note that the values of mSAC is

dependent on applied voltage, influent salt concentrations and ionic species. When using single salts (mostly NaCl) as feed water, the mSAC is easily determined, since molar mass is uniform and known. However, for a mixture of different salt ions, calculating mSAC cannot only rely on conductivity measurements of effluent stream, some analytical methods are required to determine the percentage of each ionic species [80]. In most studies, CDI cells are charged at 1.2 volts for obtaining high ion adsorption while eliminating side reactions such as water electrolysis, and the recommended concentration of feed water in CDI experiments ranges from 5 mM to 50 mM [81]. The measurements of mSAC should not include the salt concentration values during the first adsorption cycle, since micropores of electrodes are likely to achieve the full-wetting condition after a few cycles, and physical adsorption of fresh carbon materials may also lead to unreliable values. Another common mistake is to determine mSAC under constant current operation, because salt adsorption keeps happening as electron charge constantly build on the electrode surface. However, normal SAC values are still applicable when using constant current method. Suss et al. concluded the mSAC reported in numerous CDI studies, and plotted the values for different electrode material as a historical evolution trend (Figure 4) [2].

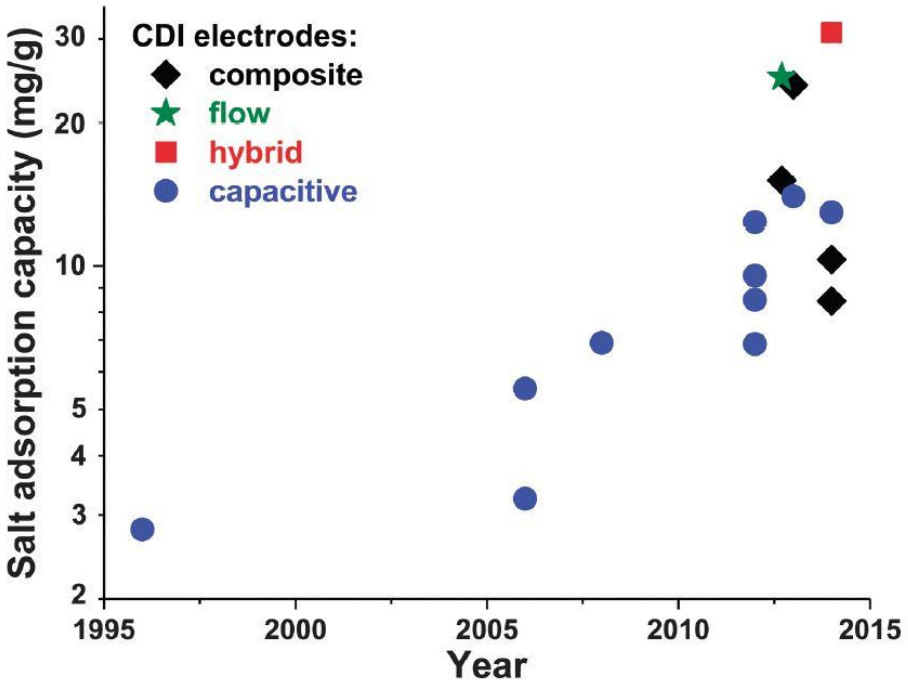

Figure 4: Maximum salt adsorption capacity (mSAC) values reported for capacitive, composite, hybrid, and flow electrodes in CDI testing from year of 1995 to 2015. (Ref. [2])

The state-of-the-art development of CDI exhibits a great improvement in salt adsorption capacity by optimizing electrode materials and system configurations. For systems using static capacitive electrodes, the mSAC values is approximately in the range between 7 to 15 mg/g according to recent CDI studies. The implementation of flow or hybrid electrodes further boost the mSAC over 20 mg/g. The theoretical predictions of mSAC upper limit for CDI system with static capacitive electrodes was made based on the capacitance theory of aqueous supercapacitors [2]. The projected maximum possible mSAC are above 30 mg/g, which implies a potential for further enhancement.

2.3.2 Average Salt Adsorption Rate

Average salt adsorption rate (ASAR) is another important parameter used for evaluating average speed of salt removal from the feed water. It is calculated by dividing the SAC values by the total charging time, and is usually reported in a standard unit (mg/g-min). ASAR is commonly calculated for CDI systems under single-pass mode, as shown in Equation 3, where $t_{c,i}$ and $t_{c,f}$ are the initial and final time of charging period.

$$ASAR = \frac{\Phi \cdot \int [c_i - c_o(t)]\, dt}{m \cdot (t_{c,f} - t_{c,i})} \tag{3}$$

This concept was used in a few CDI studies to report desalination rate [82, 83]. Later, Zhao et al. specifically defined and investigated ASAR based on the system parameters in MCDI [84]. Unlike SAC which is considered as an electrode property, ASAR is dependent on many factors in the overall system, including charging time, electrodes materials and thickness, as well as cell configuration. Therefore, it is recommended to report the values of ASAR along with pertinent experimental conditions.

The duration of charging time strongly affects the ASAR under constant voltage operation. As applying a fixed electric potential, salt concentration of feed water generally drops at a constantly decreasing rate till it reaches equilibrium. Thus, setting a shorter charging time is able to yield higher value of ASAR. Furthermore, the thickness and pore size of the carbon electrodes also has impact on adsorption rate. It has been suggested that the ion storage mechanism in sub-nanometre pores, small-sized micropores limit the

dynamic transport of ions and cause a slow response of salt removal, resulting smaller values of ASAR [85] [86]. The electrode thickness also influences the values of ASAR. Thinner electrode may contribute to shorter pathway of ion transport and commonly shows better rate capability of desalination [87]. Lastly, the cell architecture plays an important role in ASAR, with the flow-through mode, exhibiting fast response and a higher rate of salt adsorption (~1mg/g-min) [83]. The details of flow-by and flow-through architectures are described in section 2.4.1. Up to now, the highest value of ASAR reported is (~2.3 mg/g-min) when using activated carbon electrode (362 μm) in MCDI cell and applying sub-equilibrium charging time [84]. To correlate the values of SAC and ASAR, Kim and Yoon developed a plotting scheme to evaluate CDI desalination performance combines both capacity and rate, namely Kim-Yoon diagram (Figure 5) [2, 23, 88].

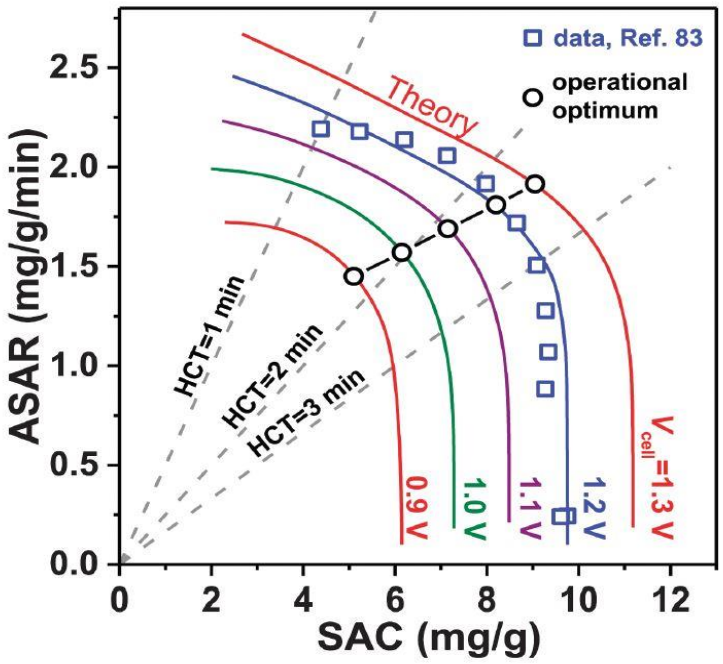

Figure 5: Kim-Yoon diagram that correlates the average salt adsorption rate (ASAR) and salt adsorption capacity (SAC). The experimental data was acquired as periods of charging (1.1~1.3 V) and discharging (0 V) are the same. Half-cycle time (HTC) is then defined as a half of the value that SAC divided by ASAR. The theoretical calculations are based on EDL and ion transport theory. (Ref. [2])

From Kim-Yoon diagram, higher ASAR at a certain charging voltage is achieved with a cost of decreasing SAC. As charging and discharging periods are symmetric, half-cycle time (HTC) is defined as a half of the ratio of SAC to ASAR. To determine the operational conditions where high SAC and SAR are obtained simultaneously, optimum HCT point can be found by maximizing the product of ASAR and SAC [89]. Based on the theoretical calculations, the optimum charging time indicated by HCT point increases with the charging voltage.

2.3.3 Charge Efficiency

Charge efficiency is a critical parameter in CDI to evaluate how efficient the electrical energy invested for removing salt ions. It is defined as the ratio of the salt ions electro-adsorbed on the porous electrodes to the electric charge transferred through electric circuits. To calculate the charge efficiency, the electric charge in coulomb is divided by Faraday's constant (F = 96485 C/mol) to express in the unit of mole. At the same time, the moles of salt ions removed during a charging cycle are determined using experimental measurements. By definition, the ratio of salt ions over electric charge yields the charge efficiency as a unitless values [2]. For a CDI system operated under constant voltage and a single pass mode, the calculation of charge efficiency is shown in Equation 4.

$$\Lambda = \frac{F \cdot \Phi \cdot \int [c_i - c_o(t)]\, dt}{\int I\, dt} \tag{4}$$

where I is instantaneous current, so that the time integral of I represents the electric charge transferred in Coulomb. Under a batch mode, the charge efficiency of CDI cell charged at a constant voltage is calculated as shown in Equation 5.

$$\Lambda = \frac{F \cdot V_s \cdot (c_i - c_o)}{\int I\, dt} \tag{5}$$

The concept of charge efficiency is firstly introduced by Johnson and Newman in 1971 to describe electrosorption behavior to EDL formation [53]. Later, specific terminology for charge efficiency was characterize [90, 91]. The symbol Λ arises in Zhao et al. where the charge efficiency is determined as a function of external voltage and salt concentration. At the same time, they used experimental data of charge efficiency to analyze the theoretical double-layer structure and effective surface area inside of porous

carbon electrodes [28]. In another study, the equilibrium charge efficiency and dynamic charge efficiency was differentiated based on whether equilibrium adsorption capacity is reached [38]. The values of charge efficiency should be less than unity, because a charged electrode is able to adsorb counter-ions from the bulk solution, and simultaneously exclude the co-ions from the EDL structure. The effect of co-ion desorption reduces the charge efficiency in normal CDI cell. At a small cell voltage, the co-ion desorption counteracts with counter-ion adsorption, which results in low values of SAC and charge efficiency. While elevating the electric potential, the counter-ion adsorption can overcome the co-ion exclusion, achieving higher charge efficiency values [28, 91].

Charge efficiency can be converted to the electric energy E_c required to remove salt ions during the charging step (kT/ion), which is described:

$$E_c = \frac{1}{2\Lambda} \cdot \frac{V_{cell}}{V_T} \tag{6}$$

where V_{cell} and V_T are the applied cell voltage and thermal voltage (25.6 mV at room temperature). At a constant cell voltage, the electrical energy consumed is inverse proportional to the charge efficiency. The specific energy consumption versus charge efficiency for CDI and MCDI cells, and the trend of experimental data from. is highly consistent with theory (Figure 6) [2, 39]. Due to the combined effects between counter-ion adsorption and co-ion exclusion, CDI has a lower charge efficiency typically ranges from 0.3 to 0.7, which results in higher energy consumption than MCDI. The ion-exchange

membranes in MCDI cells prevent co-ions leaving from electrodes, which significant enhances the charge efficiency and reduces the energy consumption.

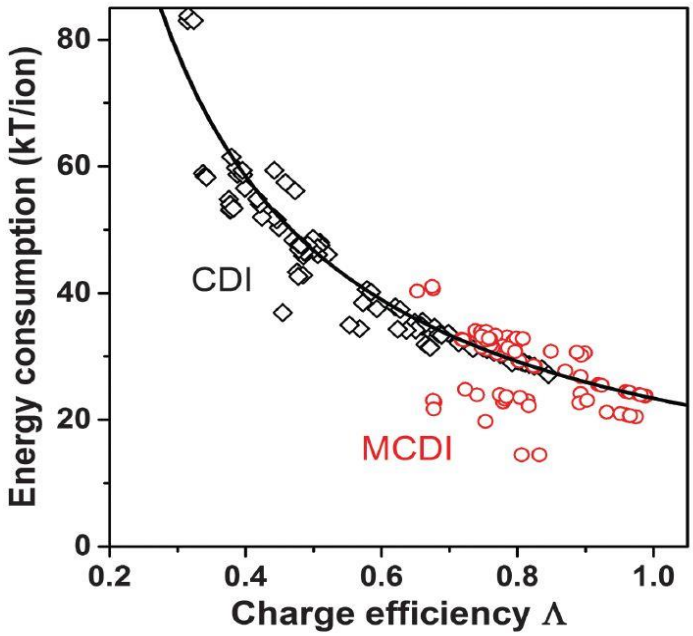

Figure 6: Energy consumption versus charge efficiency for CDI and MCDI based on experimental data. (Ref. [2])

2.3.4 Current Efficiency

In some cases of CDI operations, current efficiency λ is an alternative to charge efficiency Λ for describing how efficient the electrical energy used for desalination. This term emanates from electrodialysis (ED) [92]. Current efficiency is used for a CDI system operated under constant current and a single-pass mode. After the salt concentration reaches equilibrium, the current efficiency is calculated as shown in Equation 7. Similar to

charge efficiency, current efficiency is inverse proportional to the specific electrical energy invested for removing salt ions [2, 92].

$$\lambda = \frac{F \cdot \Phi \cdot (c_i - c_o)}{I} \tag{7}$$

Previous studies used current efficiency to evaluate MCDI or flow-electrode CDI under steady state. Extensive experimental data of MCDI shown that charge efficiency decreases as increasing salt concentration of feed water under constant voltage operation, which is possibly attributed to the reduced performance of membrane selectivity [2, 38]. However, the current efficiency of flow-electrode CDI does not exhibit a correlation with water salinity, but it became less efficient at higher current density [92].

2.4 System architecture

Cell architecture plays an important role in both electrochemical features and desalination performance of CDI. Similar to the electrochemical capacitors (or supercapacitors), the conventional CDI unit is a symmetrical cell pair where two equal porous electrodes are oppositely placed and separated with by a spacer or small distance. The carbon electrode is either brought in close contact with or directly cast on a sheet material with excellent electrical conductivity, namely current collector. The current collectors are commonly made of thin metal plate or graphite foil, allowing electric current pass to polarize two porous electrode. Unlike supercapacitor enclosing static ionic liquid,

the CDI cell enables salt water to flow along or through the porous electrodes, so that the ionic species are removed from feed stream to produce freshwater at effluent stream.

2.4.1 Two-Electrode Based CDI Geometries

Two-electrode layout is most commonly applied as constructing a CDI cell to desalinate brackish water. It contains two porous carbon electrodes that are placed in parallel. The electrodes are generally made from the same material and have equal weight and dimensions, unless the asymmetric electrode design is specified. Based on the direction of water flow relative to the electrodes, the geometry can be seen as either flow-by or flow-through mode [1, 2].

In a flow-by mode, feed water flows along with two oppositely placed electrodes, and the water flow is perpendicular to the direction of electrified field (Figure 7a). This design was first developed by Blair and Murphy in 1960, and further implemented in the following studies on electrochemical demineralization [49]. The flow-by mode is most commonly seen in CDI research due to the easy installation, and it is effective to perform CDI testing from numerous perspective, such as evaluating novel electrode materials and salt adsorption behavior. To enhance the desalination level, a stack of multiple flow-by cell pairs can be constructed in a way by placing one electrode at each two side of current collector and then assembling multiple current collectors together [15, 26, 28]. Though flow-by mode specifies water flowing along the electrodes, there are different flow patterns controlled by entrance and exit location. Besides the conventional style where feed water enters the cell at one corner of the square and leaves at the opposite corner [66], the influent

stream can enters at the center of square and radiate until it exits at four corner, or the flow direction can be reversed. This radial flow pattern is particularly favorable in multiple cell pairs [28].

Flow-through mode is another popular geometry that is firstly developed by Newman and Johnson in 1970 [53]. Here, the water flow direction is perpendicular to the electrode and parallel to that of electrified field (Figure 7b). This mode is beneficial to higher rate of salt removal, since the salt water is pressurized through the carbon material, which significantly reduces the time and scale of ion diffusion from bulk to carbon pores. Another benefit is that the flow-through architectures requires no flow channel, which minimizes the spacer thickness (~10 μm) and reduce the ohmic resistance [2]. Flow-through cell exhibit fast cell charging compared to flow-by mode [90, 91]. Flow through electrodes have been made from traditional activated carbons, as well as hierarchical carbon aerogel monolith as porous electrode [83]. Aerogels have exhibited a high level of desalination (70 mM reduction in salt concentration), and high rate of average adsorption (1mg/g-min).

Based on the two fundamental mode (flow-by and flow-through), a few novel architectures have arisen recently. An “electrostatic ion pumping” technique where the freshwater and concentrate streams are extracted at different locations has been developed [93]. It is operated by alternatively closing and opening two valves that control the effluent stream. The state of valves should coordinate with the time period of applied voltage

(Figure 7c). This design is similar to the classic technique of "parametric pumping", but employs multiple porous electrodes in the middle of chamber [54-56]. Simple CDI architecture that consists of changeable carbon rod electrode wires have also evolved [94]. Here the main objective is to avoid producing concentrate and freshwater stream from the same outlet, the assembly of electrode wires are charged to remove salt ions in one reservoir and regenerated to release salt ions in another stream. By repeating this procedures, the freshwater can be continuously produced in one stream from the feed water, while the other stream becomes more concentrated in salt ions (Figure 7d).

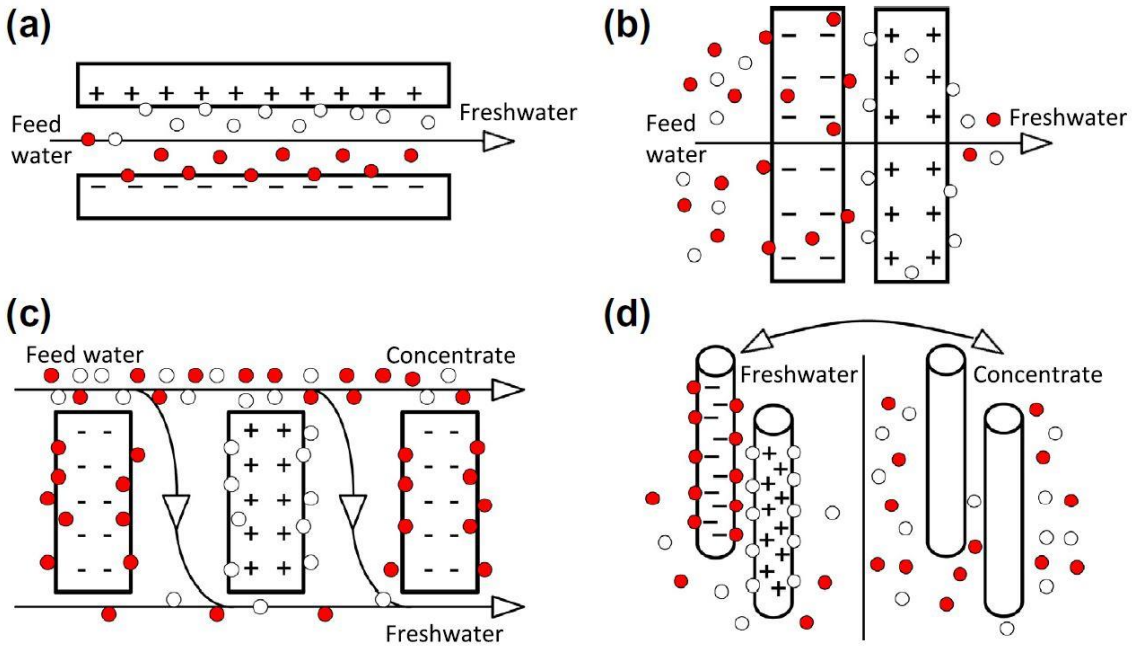

Figure 7: Four types of CDI cell geometry (Ref. [1]): (a) Flow-by geometry (b) Flow-through geometry (c) Electrostatic ion pumping (d) Carbon rod electrode wires.

2.4.2 Membrane Based CDI Geometry

Introducing ion-exchange membranes (IEMs) into CDI leads to significant improvement of desalination performance. The IEMs are placed in front to the porous carbon electrode to construct a modified CDI structure, namely membrane capacitive deionization (MCDI). IEM contains covalent-bond groups such as sulfonate or quaternary amines, allowing for the access of either positive or negative ions [1]. Therefore, the IEMs are classified to cation exchange membrane (CEM) and anion exchange membranes (AEM). The common MCDI cells are constructed by placing a CEM onto one carbon film electrode and an AEM onto the other one. As applying voltage difference over two electrodes, the counter-ions, the ions carrying opposite charge to the polarized electrode, are immobilized inside of porous electrodes. In the meantime, the co-ions with the same charge sign as the electrodes are expelled to release back into the flow channel. For instance, the cations such as Na^+, is the co-ions in the anode (negative electrode) and counter-ions in the cathode (positive electrode). However, as including IEMs into CDI cell, the co-ions excluded from EDL are confined in the macropores of electrodes due to ion selectivity of membranes. As a result, additional counter-ions in the bulk stream are attracted based on charge neutrality. The elimination of co-ion exclusion effect significantly enhances the SAC and charge efficiency of MCDI [39]. Lee et al. for the first time demonstrated the MCDI structure in 2006 and shown the salt removal rate of MCDI is 19% higher than conventional CDI cells [43]. Since then, numerous studies have focused on MCDI from different perspective including membrane materials, theoretical understandings and operation optimization [32-43, 84].

Another advantage of MCDI is that the voltage polarization of cell can be reversed during ion desorption process. The conventional CDI cells are discharged by reducing or short-circuiting the electrical voltage. If the voltage shift to negative, the salt ions are released back into the bulk solution and subsequently adsorbed on the opposite carbon electrode, which fails to recover the ion storage capacity. However, the AEM and CEM included in MCDI cell makes each electrode accessible to only one type of ions (cations or anions), so reversing the electrical polarization to can fully regenerate carbon electrodes. It was found that discharging MCDI cell with reversed voltage gains higher values of SAC and charge efficiency compared to zero-voltage discharge [1]. Through optimizing the operational conditions, the highest reported value of ASAR (2.3 mg/g-min) and with nearly a 20 mM decrease in salt concentration was observed [84]. Energy consumption of MCDI is lower than other state-of-the-art desalination techniques (less than 0.6 kWh/m^3 specific energy) [38]. MCDI achieves much higher charge efficiency than the conventional CDI devices, for the same amount of salt removal, because MCDI has lower resistive losses and better ion competition processes (co-ion exclusion) [2, 28].

2.4.3 Flow-Electrode CDI Geometry

Flow-electrode capacitive deionization (FCDI) is another novel structure that replaces the solid film electrode with suspended carbon slurry (Figure 8). This concept is based on the design of electrochemical flow electrode which has also been demonstrated in semi-solid batteries and supercapacitors. Due to the non-finite surface area, this approach has the potential to perform high concentration desalination processing, including

seawater desalination. Initial works in this area prepared the flowing electrode with 5% weight of activated carbon and also combined IEMs, to separate a feed water channel. This study was capable of removing more than 95% salt ions from highly concentrated NaCl solution (32.1 g/L) [45]. The salt removal rate, in the meantime, is measured to be 0.411 mg/min-cm^2. Later a FCDI system without using IEMs, was developed and demonstrated high gravimetric capacitance and low cell resistance [46]. Another important study by explored the ion recovery and energy storage of FCDI. Two operational modes were specified based on the state of valve: isolated closed cycle mode and short-circuited close cycle mode. The difference in salt removal and current between those modes explained the ion storage in the flow electrodes and energy recovery during discharging step. They also reported the energy recovery from applied electrical energy is around 20% [44].

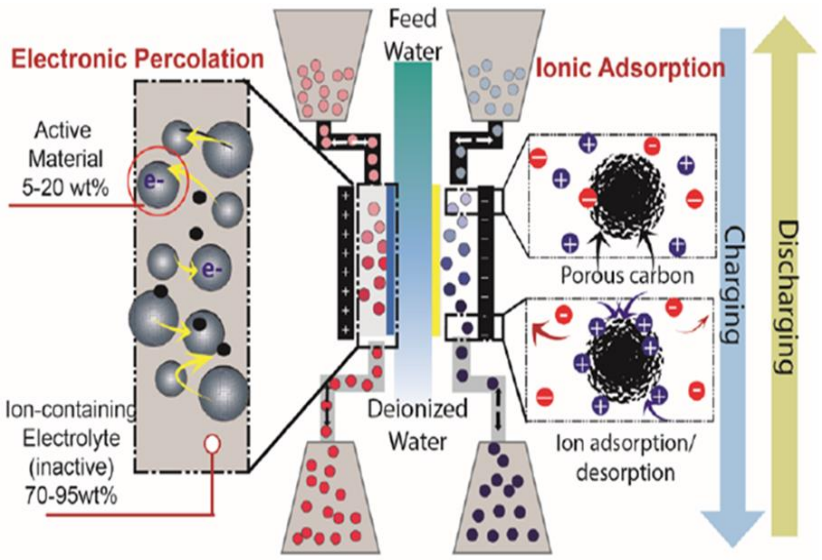

Figure 8: Schematics of flow-electrode CDI. The suspended carbon slurry (5-20 wt.% of activated carbon) is used as flowing electrodes for continuous desalination.

The major advantage of FCDI over other common structures is suspended carbon electrode with unlimited salt adsorption capacity. FCDI also allows for continuous charging for desalination and avoids intermittent operation procedures.

2.5 Theory of Electrical Double Layer (EDL)

The Electrochemical Double Layer (EDL) at electrified interface, is important in many electrochemical devices, such as batteries, electrowetting devices, or deionization systems [95]. Since the German physicist, Herman von Helmholtz first presented the concept of double-layer capacitance in 1853 [96], a great number of researchers have focused on describing the properties and structure of EDL, contributing the development of the corresponding applications like electrochemical capacitors, capacitive mixing and deionization. The EDL, forms at the interface between the solid electrode and ionic electrolyte, when electrical voltage difference is applied. When electron charges start to flow through an external circuit, surface charge (either positive or negative) accumulates at the negative or positively biased electrode due the electric field in the electrolyte solution. Therefore, the double layer describes the ionic charge distribution and resulting voltage drops which results due to this ionic charge distribution at a surface.

2.5.1 EDL Structure

The double layer developed at an electrified interface consists of a compact layer (inner and outer Helmholtz layers) and a diffuse layer (or Debye layer) [97]. The inner

compact layer describes the region affected by strong electrostatic force. The solvent molecules and ions specifically adsorb on the electrode surface. Based on the distance at which the adsorbed ions and solvated ions approach to the metal, the compact layer can be divided into the inner and outer Helmholtz layer [97]. Within the compact layer, the Faradaic reaction can take place at an effective electrostatic potential, whose magnitude is smaller than the applied electrode voltage [98]. When moving along the electrified field, the interactions between the solvated ions and charged electrode is no longer dependent on the chemical properties of the ions. Those ions non-specifically adsorb to the polarized surface, and the region where those ions distribute is referred as Diffuse Layer. The diffuse layer depicts the gradient of the charge distribution extended from outer Helmholtz layer toward the bulk solution, which results from the coulombic forces and random thermal agitation. In the diffuse layer region, the concentration of the solvated ions will decrease, as the distance from the electrode increases. The thickness of diffuse layer is strongly dependent on the applied electrode voltage and the bulk concentration of ionic charge. For high electrolyte concentration greater than 10^{-3} M, the thickness of electrolyte is on the order of nanometer [99].

2.5.2 EDL Theoretical Models

The Helmholtz model described EDL at the interface between solid metal and electrolyte base on charge neutrality. With excess electron charges distributed at the metal surface, the counter-ions in the solution are strictly adhered on the other side of surface, establishing a two-sheet of charge separated by order of molecules [96]. However, later

studies on EDL shown that the ionic charges in electrolyte solution were not strictly confined to the electrode surface while applying an electrical polarity. The charge carriers are under the influence of the electric attraction and exclusions, and in the meantime performs randomly thermal motion. This interaction leads to the formation of a finite-thickness region to counterbalance the excess electron charges.

To reveal the ion distribution more accurately, Gouy and Chapman proposed the concept of the diffuse layer and performed theoretical modeling based on statistical and mechanical principle. Based on their theory, the thickness of the diffuse layer depends on the concentration of the electrolyte and applied potential. Higher applied potential leads to greater charge density on the metal side, creating a stronger electrostatic force to attract ionic charge carriers. In such way, the diffuse layer shrinks, consequently increasing the capacitance of electrodes. Similarly, a higher concentration of electrolyte provides more charge carriers to compensate the electric polarity, which decreases the thickness of diffuse layer and results in a greater value of capacitance. However, the Gouy-Chapman model overestimated the increase in differential capacitance with surface charge density, and the major reason is that the ions in the electrolyte are treated as point charge that can unlimitedly approach to the metal surface [97]. Although, small salt concentration and charge density leads to expansion of diffuse layer where ion size has small effect. For high concentration and charge density, the ion size cannot be overlooked. Stern modified the EDL model by including an imaginary plane to account for ion size and a layer of solvent on the electrode surface [100]. The corrections made on the electrostatic potential and

differential capacitance is presented in the Gouy-Chapman-Stern (GCS) model, which is extensively applied to following EDL modeling works.

2.5.3 EDL Theories in CDI

Since EDL formation at carbon surface is the fundamental of salt electrosorption in CDI, many theoretical works focused on developing EDL models to characterize the actual mechanism. Biesheuvel theoretically investigated the thermodynamic cycle for CDI and analyzed different EDL models for computing input and output electrical work through a reversible charging-discharge cycle [101]. The Gouy-Chapman model and GCS models were applied to demonstrate the change in surface charge with respect to the cell voltage. Moreover, the Carnahan-Starling (CS) equation was used to account for the ion size constraints and further combined with GCS model for more realistic characterization at high salt concentration. In all of those models, the salt adsorption is assumed as an ideal non-Faradaic process within the monovalent ionic solution. The double layer voltage V_{dl} is equal to half of the overall cell potential, and it consist of the diffuse layer voltage V_d and stern layer voltage V_{st}, which is described in Equation 8.

$$V_{dl} = V_d + V_{st} = \frac{1}{2} V_{cell} \tag{8}$$

Based on the Gouy-Chapman model, the diffuse layer voltage is dependent on the surface charge density σ in unit of number per electrode area and ionic strength c_s in unit

of number per solution volume. The relationship is shown in Equation 9, where κ is the inverse of Debye length and V_T is the thermal voltage.

$$\sigma = 4\frac{c_s}{\kappa} \cdot \sinh\left(\frac{1}{2} \cdot \frac{V_d}{V_T}\right) \tag{9}$$

The thermal voltage (25.6 mV at room temperature) is computed by multiplying Boltzmann constant k_B with temperature T, divided by the elementary charge ($V_T = k_B T/e$). The Debye length is related with ionic strength c_s and Bjerrum length λ_B (0.72 nm at room temperature). The calculation is exhibited in Equation 10, where ϵ_r is the dielectric constant of salt solution.

$$\kappa^2 = 8\pi c_s \lambda_B = \frac{8\pi c_s e^2}{k_B T \epsilon_r} \tag{10}$$

The Gouy-Chapman model only takes the diffuse layer into account (V_{dl}=V_d), and the salt ions are considered as point charge. Therefore, the surface charge density plotted based on Equation 2 exponentially increases with cell voltage, which is not consistent with real case. By including the Stern layer voltage, GCS model significantly improves the accuracy of the change in surface charge. The Stern layer capacity C_{st} can be assumed as a constant value, like 2 F/m^2, so the Stern layer voltage is calculated as shown in Equation 11.

$$V_{st} = \frac{\sigma \cdot e}{C_{st}} = 4\frac{e c_s}{\kappa C_{st}} \cdot \sinh\left(\frac{1}{2} \cdot \frac{V_d}{V_T}\right) \tag{11}$$

Although GCS model can realistically predicts the double layer behavior, the theoretical values of salt concentration within Stern layer are also impractical. Biesheuvel further made corrections by combining GCS models with Carnahan-Starling (CS) equation, in order to consider the ion volume interaction in diffuse layer. The CS equation uses off-lattice concept to visualize the volume constraints in mixtures of hard spheres. With this modification, the salt concentration predicted at Stern layer is more realistic compared to the bulk solution. The numerical schemes of GCS-CS model is shown in Ref 103.

In another study, Janssen et al. investigated the temperature effect on double layer voltage based on a modified Poisson-Boltzmann theory [102]. To derive the expression of EDL voltage, they neglected the complex porous structure of carbon electrodes and assumed one electrode simply contains two parallel plane surfaces which separated by a distance on the order of nanometer. Additionally, 1:1 monovalent salt solution is assumed to get contact with two symmetrical electrodes. By numerically solving a modified Poisson Boltzmann theory, they derive the double layer voltage that is not only dependent on surface charge and ionic strength, but also changes with temperature. Such dependence can be seen in Equation 12.

$$V_{dl} = \frac{2k_B T}{e} \sinh^{-1}\left(\sqrt{\frac{\exp\left[2\gamma\left(\frac{c_s}{c_s^*}\right) - 1\right]}{2\gamma} + \frac{4\pi e\sigma R}{\epsilon_r}}\right) \tag{12}$$

This modified Poisson-Boltzmann theory applies a lattice gas model, so the lattice spacing R is used to set the size of ionic species (R = 0.34 nm), and γ is the packing parameter, which is calculated based on R. To separate the linear and non-linear screening region, a cross-over charge density c_s^* is used as a correction parameter. The calculations of R and c_s^* are shown in Equation 13.

$$\gamma = \frac{8\pi}{3} \cdot c_s \cdot R^3 \qquad c_s^* = \sqrt{\frac{2c_s}{\pi \lambda_B}} \tag{13}$$

From Equation 5, the double layer voltage V_{dl} can be plotted with respect to temperature using different surface charge σ and ionic strength c_s. The theoretical results indicate higher surface charge and lower salt concentration leads to greater values of V_{dl}. It was found that double layer voltage also increases with temperature. Moreover, the authors evaluated the theoretical energy consumption throughout an intermittent CDI cycle based on the EDL modeling. They illustrated that it is more energy efficient to desalinate cold salt water than the hot brine. However, adjusting temperature in the operation cycle is possible to achieve additional energy saving [102].

CHAPTER 3. METHODS

3.1 Electrode Fabrication

Carbonaceous materials are popular for making porous electrodes in CDI due to high specific area, electrical conductivity and Faradaic resistance. The activated carbon film electrodes are fabricated by mixing activated carbon powders (Sigma-Aldrich, USA), carbon black (2-12 μm, Sigma-Aldrich, USA), and polytetrafluoroethylene (PTFE, 60% wt. dispersion in H_2O, Sigma-Aldrich, USA), with a weight percentage of 85:5:10. The major component, activated carbon, has extremely high surface area (1000-3500 m^2/g), providing large adsorption spaces for salt ions, while the carbon back as a minor addictive can increase the electrical conductivity of the carbon electrodes. PTFE is a polymer material used for binding the carbon particles and improving the mechanical strength. The three constituents were dissolved in ethanol and stirred on a Hot Plate for homogeneous dispersion. As soon as a viscous mixture formed, it was flattened and surfaced to a carbon film using an electric roller press (MTI Corporation, USA). The film thickness was adjusted to around 0.3 mm. For enhanced mechanical strength and cycling stability, the film was heat-treated in an oven for 4 hours at 150°C. After that, it was cut into the square electrodes (2×2 cm^2) for the use of CDI and MCDI experiments (Figure 9a).

The porous structure of carbon film electrodes was detected by Scanning Electron Microscope (LEO 1530 SEM). The carbon surface was observed at resolutions of 2 μm and 10 μm. Since the activated carbon film were fabricated without templating process, the electrode surface exhibited irregular pattern of pore structure and wide range of pore size (Figure 9b).

(a)

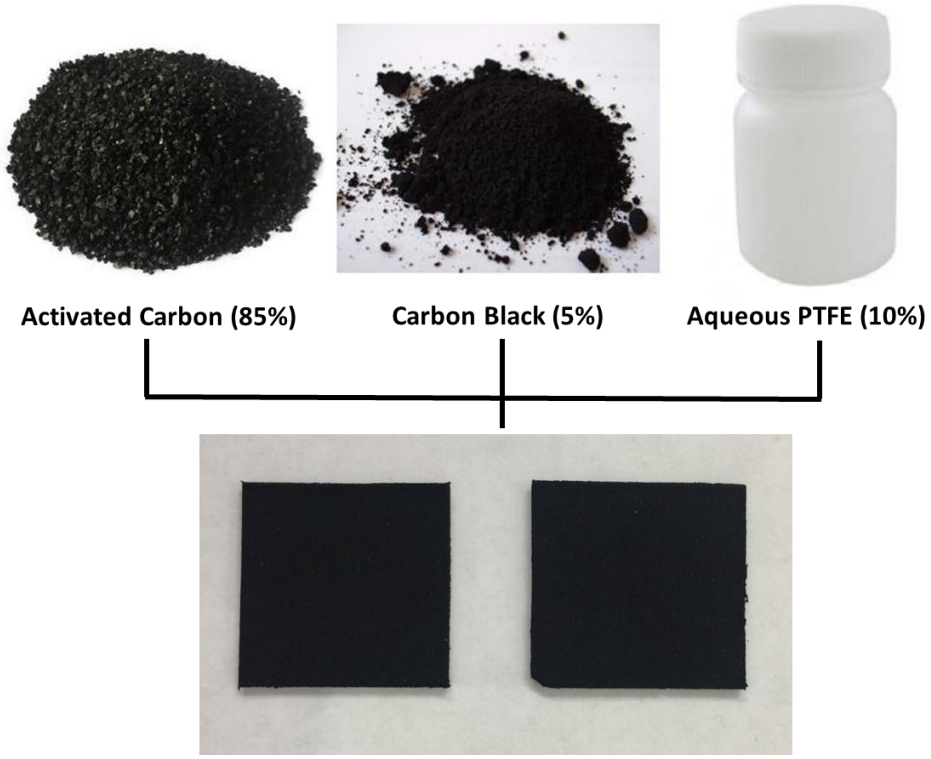

(b)

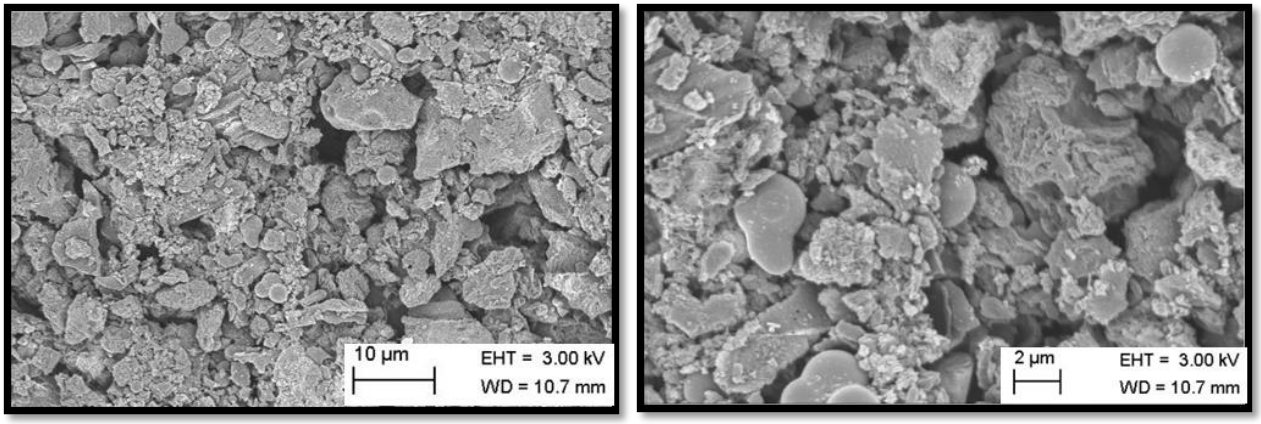

Figure 9: The components and SEM images of activated carbon electrodes. (a) Three components used to fabricate the carbon film electrodes (activated carbon powder, carbon black, PTFE) and their weighting percentage. (b) SEM images of electrode captured at 2 different resolutions.

3.2 Experiment Setup

This section presents the CDI and MCDI cell used in the bench-scale experiments, as well as the overall system configuration. The cell is essentially a flow device that is assembled from several individual components, and the overall setup is designed to support batch-mode desalination tests and electrochemical characterizations of the cell.

3.2.1 CDI and MCDI Cell Assembly

The CDI cell consists of two polycarbonate end-plates, two titanium current collectors, two activated carbon electrodes, and one silicone gasket (δ = 1mm, McMaster-Carr, USA) in which the flow channel was cut through. All the components are sandwiched with the symmetry of the gasket positioned in the middle, where the salt solution can pass through and contact with two electrodes. The CAD drawings and actual view of CDI cell assembly are presented (Figure 10). The function of end-plates is locking in-between components and applying high pressure to avoid water leakage. Two titanium current collector has high electrical conductivity, allowing for electron charge transfer with small resistance. The activated carbon electrodes are strictly attached to the inner side of current collectors and separated by the flow channel. All the components are symmetrically stacked together and compressed by threaded rods and wing nuts. To prevent short circuit inside of the cell, hot-shrinkage tubing is used for covering the middle surface of the rods that is in contact with salt solution.

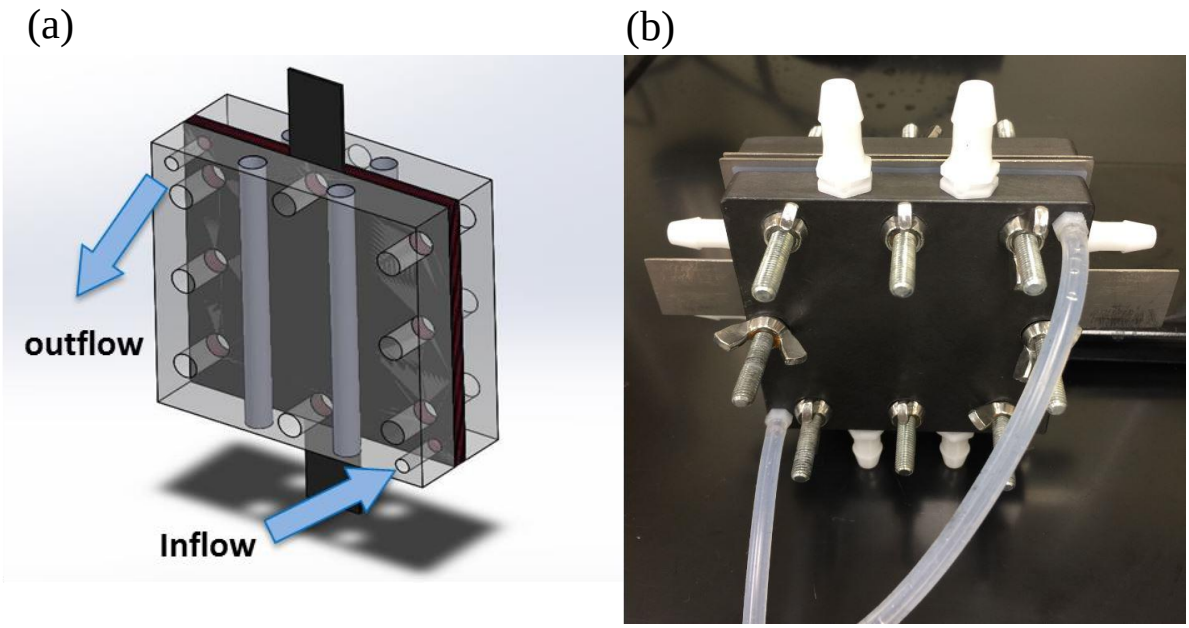

Figure 10: (a) The CAD design of CDI cell consists two end-plates, two current collectors, two activated carbon electrodes and one silicone rubber gasket. (b) The actual assembly of CDI cell.

MCDI cell is assembled based on the same geometry of CDI cell, but includes ion exchange membranes (IEMs). Two membranes (Selemion, AMV, and Selemion CMV, δ = 110 μm, AGC Engineering, Japan) are placed in front of two activated electrodes, making each electrode only accessible to either cations or anions. Note that AEM and CEM should be consistent with cathode and anode respectively, otherwise the salt adsorption cannot take places while applying positive voltage.

3.2.2 System Configuration

Because of the single-stack cell and small size of electrode, the CDI or MCDI experiments are performed in a batch mode. A flow vessel contains the sample salt solution with a certain volume (25 mL), and the salt concentration is measured by a conductivity meter (Orion Star A215, Thermo Scientific) with a probe immersed into the flow vessel. The four sensors of the probe are fully submerged in the salt solution for accurate measurements. The conductivity values measured in the bulk solution can be translated to the salt concentration based on a calibration curve (Figure 11).

The salt solution is pumped into the cell through the inlet tubing with a flow rate of 10 mL/min, and then returns back to the same flow vessel through the outlet tubing, completing the batch cycle. For sufficient contact between salt water and carbon electrodes, the salt solution enters the cell at the bottom corner of the end-plate and leaves from the opposite corner at the top. The flow vessel sits on a hot plate, allowing for constantly stirring the solution and controlling the water temperature with assistance of a thermocouple. The potentiostat alligators are connected with two current collectors of CDI cell for applying a voltage difference. For MCDI experiments, the working electrode is connected with the current collector at the same side of AEM, because it is losing electron charge, which allows anions passing through the membranes to form EDL. Similarly, the counter electrode is connected to the same side of CEM. The schematic view and actual layout of the overall system are used to demonstrate the overall system configuration (Figure 12a and b).

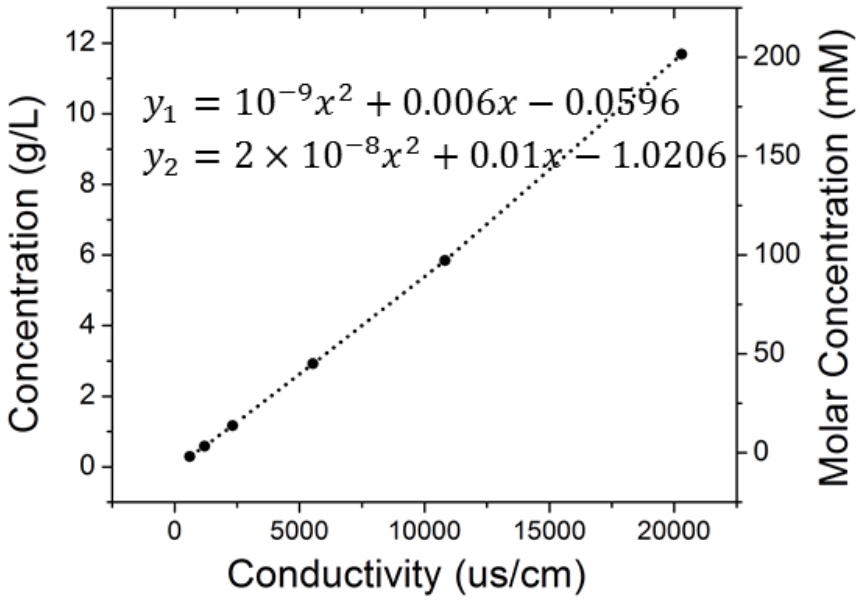

Figure 11: The calibration curve and fitting equation for converting conductivity values to mass concentration and molar concentration.

(a)

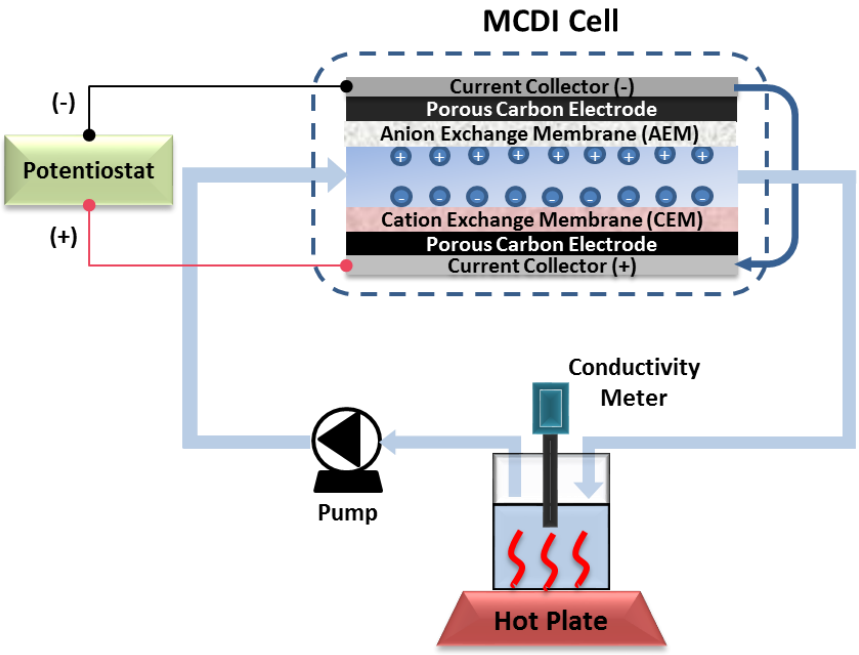

(b)

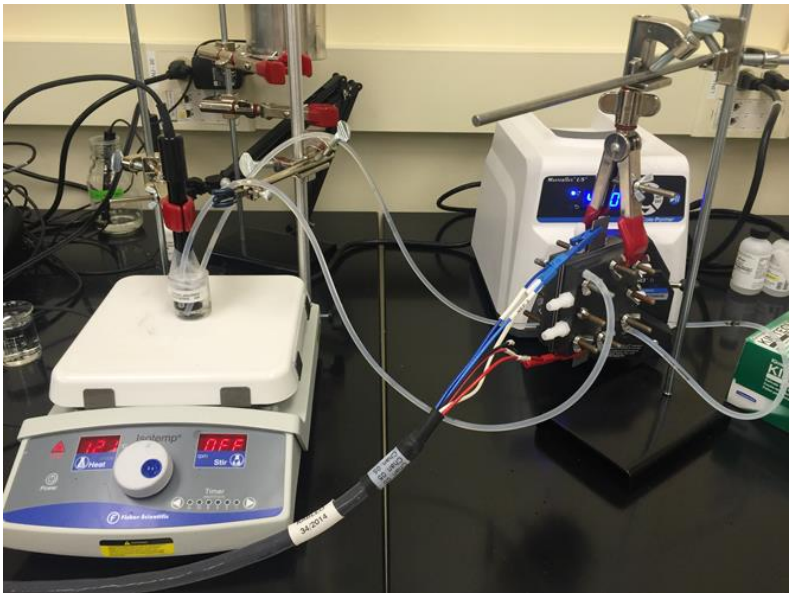

Figure 12: (a) Schematic view of the overall experiment setup. The CDI or MCDI cell is operated in a batch mode, where the sample solution is pumped from one reservoir to the cell and returns back into the same reservoir. A conductivity probe is submerged into the bulk stream to measure the salt concentration. (b) The actual layout of the overall system in CDI or MCDI experiments

3.3 Experiment Techniques

The general CDI and MCDI experiments are performed with assistance of a potentiostat. This section concludes 4 electrochemical techniques used in this study for different experimental objectives. Cyclic Voltammetry (CV) and Electrochemical Impedance Spectroscopy (EIS) are two methods used to characterize the electrode capacitance and cell resistance. While the desalination performance is determined through intermittent charging-discharge cycles, where Chronoamperometry (CA) or Chronopotentiometry (CP) are used to control the voltage and current.

3.3.1 Cyclic Voltammetry

The Cyclic Voltammetry (CV) functions by scanning the potential of a stationary working electrode using a triangular potential waveform. The potential sweep range and sweep rate are preset in potentiostat. As the CV starts, the potentiostat measures the current at the electrode interface. Since ideal CDI is a non-faradaic process, CV is used to determine the specific capacitance of the activated carbon electrodes, which potentially reveals the charge storage capacity in EDL. It is important to note that CV is not applicable to MCDI system, since ion transport is blocked by membranes as reversing the electrical polarization. Therefore this study mainly used CV technique to test CDI cell.

The voltage was cyclically swept in a range from -1.0 to 1.0 V at different scan rates (v = 2 mV/s, 5 mV/s, 10 mV/s) to collect the current response of CDI cell (Figure 13).

The CV diagram of the ideal electrochemical capacitors should exhibits a perfect rectangular shape. However, enclosed curves captured for CDI cell are stretched due to the resistive elements of the internal cell. The shape of the CV curve is also dependent on the scan rate. Increasing the potential sweep rate yields the higher current range, but at the same time results in less polarizable behavior. From the data in CV diagram, the specific gravimetric capacitance C_{sp}, the capacitance per mass of the activated carbon electrodes, is calculated based on Equation 14, where m is the average mass of one carbon electrode, i is the instantaneous current value with respect to the voltage position, and ΔV is the voltage sweep window [103].

$$C_{sp} = \frac{2}{v \cdot m \cdot \Delta V} \int i \, dV \tag{14}$$

The salt concentration and potential sweep rate strongly influences the values of specific capacitance. As using 500 mM NaCl solution, the specific capacitances at the scan rate of 2, 5, and 10 mV/s are calculated from Equation 14 (C_{sp} = 117.61 F/g, 94.58 F/g, and 68.17 F/g).

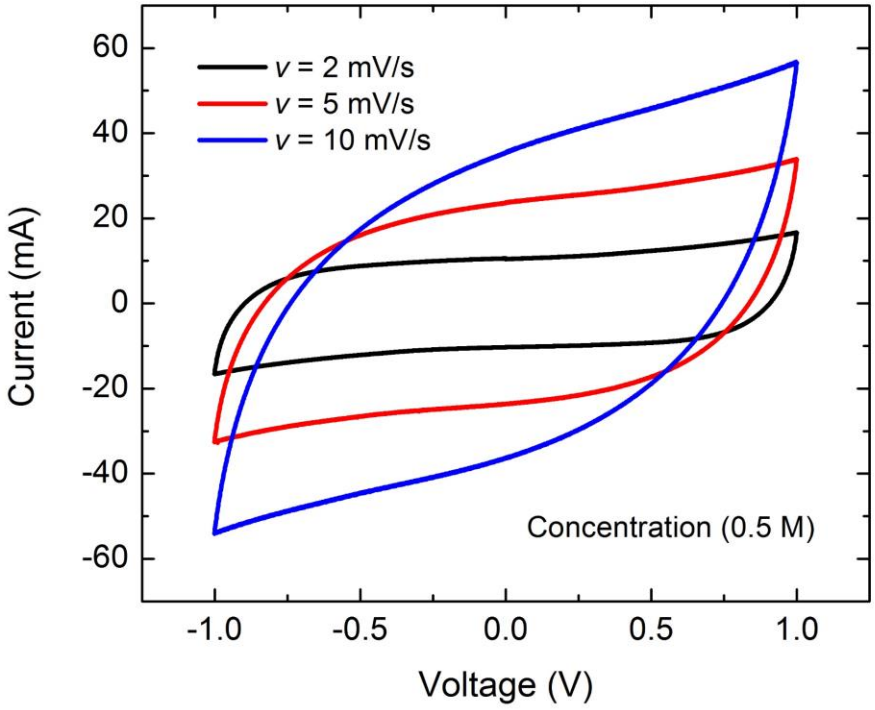

Figure 13: Cyclic Voltammetry (CV) diagrams obtained at 3 different flow rate (v = 2, 5, and 10 mV/s), and concentration of salt water in CDI cell is 500 mM.

3.3.2 Electrochemical Impedance Spectroscopy

The principle of Electrochemical Impedance Spectroscopy (EIS) is to perturb the testing devices with an alternative signal at different frequency and to collect the corresponding system changes with perturbation at the steady state. It is used to determine the capacitive and resistive elements of electrode-electrolyte interface and the entire cell based on a Nyquist diagram generated. The Nyquist diagrams of CDI and MCDI cell at different operational conditions (salt concentration and temperature) are generated within the frequency range from 200 kHz to 10 mHz.

The electrochemical features of the internal cell structure are embodied in the Nyquist diagram, represented as a depressed semicircle along with an inclined line (Figure 14). The starting point of the curve at high frequency indicates the internal resistance R_s, including Ohmic resistance from electrodes, membranes, and electrolyte. The semicircle provides the information regarding to the charge transfer resistance R_{CT} and double-layer capacitance C_{DL}. Followed by the semicircle, an inclined tail at low frequency is related with the ion transport dynamics [104]. To quantitatively evaluate those resistive and capacitive elements, an electrical circuit model is used for simulating the curve which matches the experimental data. The electrical components in the circuit correspond to the physical and chemical characteristics of the CDI or MCDI cell, which describes how the system changes with dependent variables.

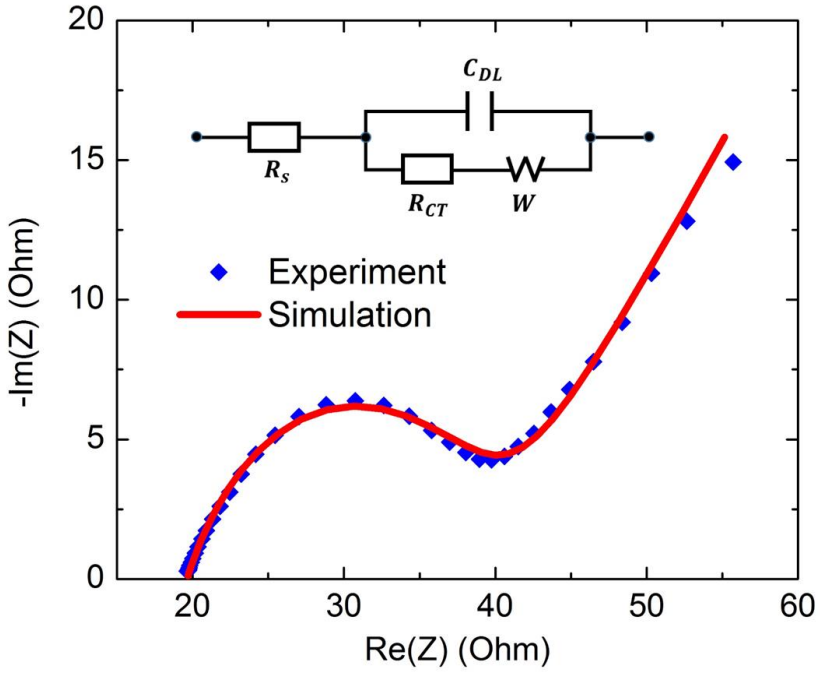

Figure 14: The experimental Nyquist diagram of MCDI cell generated by EIS technique and the corresponding fitting curves simulated based on an equivalent electrical circuit. (c=5 mM and T=21°C)

3.3.3 Chronoamperometry

Chronoamperometry (CA) functions by applying a constant voltage to the testing device and collecting the current response at the same time. CDI operates in a charging-discharge cycle where porous carbon electrodes remove salt ions from feed water during the charging process and release ions to regenerate its adsorption capacity by discharging the cell. In a constant voltage operation mode, a positive voltage is applied by CA technique to charge the CDI cell. After a certain time, discharging process can take places by setting a reduced voltage or short circuiting the cell (0 volts). Note that the CDI cell is unable to discharge at a negative voltage, since the salt ions released from one electrodes are re-adsorbed to the opposite electrode. However, the electrical polarization can be reversed for MCDI cell during the ion desorption process, due to the ion selectivity of IEMs.

Here, the CDI and MCDI cells are charged at 6 different voltages (V = 1.0, 1.2, 1.4, 1.6, 1.8 and 2.0 volts) to desalinate 5 mM NaCl solution. After a certain period, the CDI cell is discharged at 0 volt, while MCDI is discharged at a voltage with same magnitude but negative sign of the charging voltage. Additionally, the constant voltage experiments use symmetrical operation condition, where the charging and discharge periods are set to be the same (1 hour). Throughout the complete cycles, the potentiostat records the current values while the conductivity meter detects the change in salt concentration (Figure 15). Since one objective of this study is to determine the temperature effect on salt removal, the ion adsorption-desorption cycles for each charging voltages are operated at 2 different temperature (21°C and 35°C).

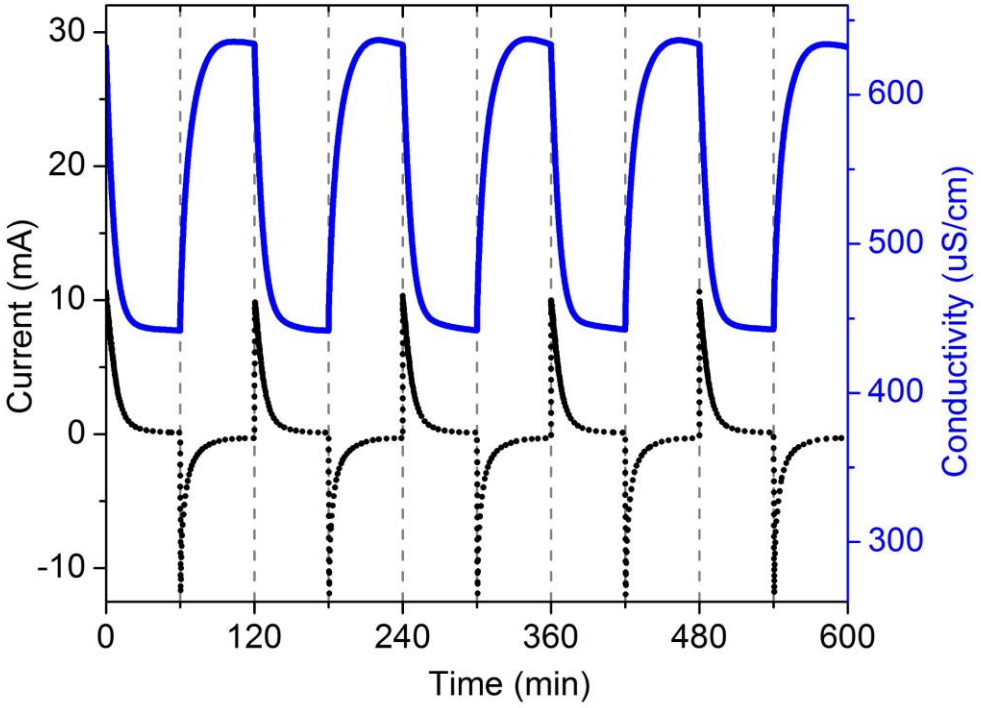

Figure 15: The charging-discharge cycles of MCDI cell operated by CA technique (constant voltage mode). The current response and conductivity changes are demonstrated. Initial concentration of NaCl solution is 5 mM, and the cell was charged and discharged at 1.2 V and -1.2 V.

Based on the current response and conductivity changes, various important desalination parameters are determined, such as salt adsorption capacity (SAC), average salt adsorption rate (ASAR), and charge efficiency (see section 2.3). The conductivity values are converted to the salt concentration using a calibration curve, so that the amount of salt removal during one charging cycle is determined. To calculate the charge efficiency, the coulomb of electron charge transferred are computed by the integral of current over time.

3.3.4 Chronopotentiometry

Unlike CA technique, Chronopotentiometry (CP) operates by applying constant current to the testing cells and capturing the voltage changes. Most of CDI studies uses constant voltage mode to perform desalination experiments, but constant current mode recently has drawn much attention, since it is superior over constant voltage mode regarding to the practical requirements. In a single-pass CDI system, constant current operations keep the salt concentration of effluent stream at a constant value, and is able to adjust the desalination level by changing the current settings [1]. Moreover, this method is more promising to reduce the overall energy consumption [39]. From this perspective, CP technique is applied to the MCDI cell to investigate the effect of varying temperature and salt concentration on energy recovery.

In traditional charging-discharge cycles operated by CP method, the MCDI cell is charged at 1.5 mA and discharged at 0 mA, and the time period of each step is set to be the same (45 min). The voltage response is captured throughout the cycles, and the conductivity values are measured at the same time to monitor the change in salt concentration (Figure 16a). In this study, a novel 3-stroke cycle is introduced under constant current methods for the energy analysis. The MCDI cell is charged at 3.0 mA to desalinate 5 mM NaCl solution until the cell voltage reaches 2 volts, which is followed by an open-circuit voltage (OCV) technique for 10 minutes. At the beginning of the OCV mode, another NaCl solution reservoir is replaced to determine the effect of temperature and ion concentration on the energy recovery. Three different salt concentration (0.5 mM,

5 mM, and 500 mM) are prepared for open-circuit flushing and discharging the porous electrodes. Moreover, the brine stream at different temperature (21°C, 35°C and 50°C) were used to include the thermal influence. Once OCV step completes, the MCDI cell is discharged at -1.5 mA until the cell voltage reaches 0 volts. (Figure 16b)

While the ion adsorption process requires the electrical energy input into the system, discharging the cell for regenerating carbon electrodes is able to recover a portion of energy. To evaluate the net electrical work, the current response is recorded throughout the 3-stroke cycle. Based on the experimental measurements, the energy consumed and recovered (E_c and E_d) is calculated by integrating the power over the time period of ion adsorption and desorption respectively. Given that charging current (I_c) and discharge current (I_d) are maintained constant, the net electrical energy (E_{net}) throughout the cycle is computed as Equation 15, where $t_{c,i}$ and $t_{c,f}$ denote the moments that constant current is applied and removed during the charging step, while $t_{d,i}$ and $t_{d,f}$ represent the same meaning but for the discharge interval.

$$E_{net} = E_c - E_d = I_c \cdot \int_{t_{c,i}}^{t_{c,f}} V\, dt - I_d \cdot \int_{t_{d,i}}^{t_{d,f}} V\, dt \tag{15}$$

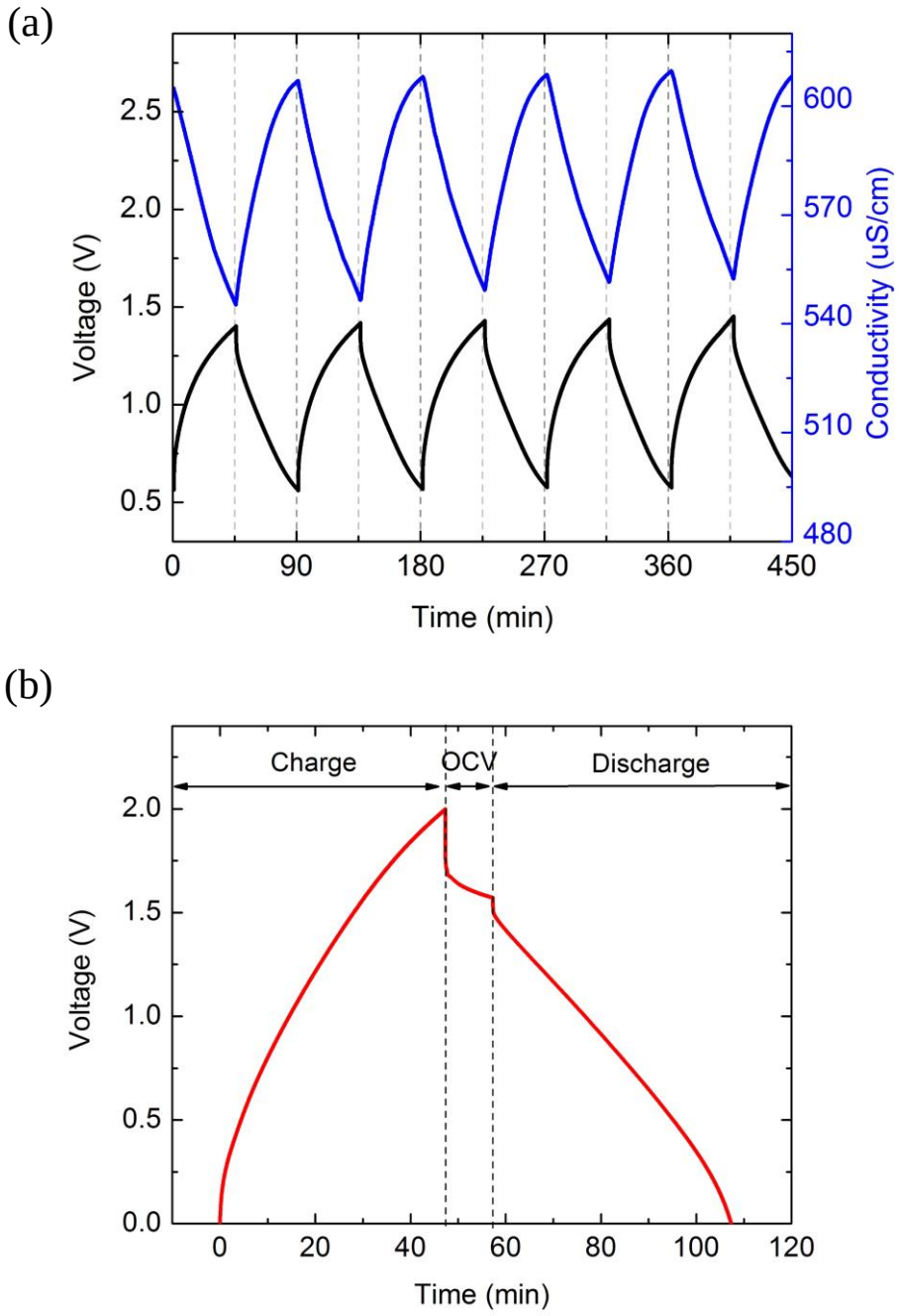

Figure 16: (a) Traditional charging-discharge cycles of MCDI cell operated by the CP technique: The cell is charged at 1.5 mA and discharged at 0 mA, while the initial ion concentration of NaCl solution is 5 mM. (b) The voltage response in a 3-stroke intermittent cycle: an OCV flushing mode is interposed between the charging (3 mA) and discharge (-1.5 mA) steps.

CHAPTER 4. RESULTS AND DISCUSSION

4.1 Theoretical Modelling

To explore the effect of temperature and salt concentration on CDI performance, theoretical approach was applied to evaluate the EDLs sensitivity to temperature. The Gouy-Chapman-Stern (GCS) model, described in section 2.5, was used to probe the electric double layer dynamics. Based on Poisson-Boltzmann equation and GCS model, the EDL voltage is derived as shown in Equation 16.

$$V_{DL} = \frac{L\sigma}{\epsilon_0 \epsilon_r} = \frac{2k_b T}{e} sinh^{-1}\left(\frac{\sigma}{\sqrt{8c_s N_A \epsilon_0 \epsilon_r k_b T}}\right) \quad (16)$$

where L is the EDL effective thickness, σ is surface charge density, ϵ_0 is electric constant, ϵ_r is the relative dielectric constant, k_b is Boltzmann constant, T is temperature in Kelvin, e is the elementary charge, c_s is the ionic strength, and N_A is Avogadro's constant. Note that the dielectric constant ϵ_r describes the permittivity of salt solution in a CDI cell, and directly affects the amount the charge stored in EDL. It is dependent both on temperature and salt concentration. Here an experimental fitting curve is used to calculate ϵ_r in different conditions, which is shown as $\epsilon_r = (87.88 - 0.39T + 0.00072T^2) \times (1.0 - 0.2551c_s + 0.05151c_s^2 - 0.006889c_s^3)$ [105]. The EDL potential as a function of temperature and concentration (Appendix A1) show distinct relationships. Specifically, as the temperature increases, the voltage increases, however voltage also increases with decreasing concentration (Figure 17a and b).

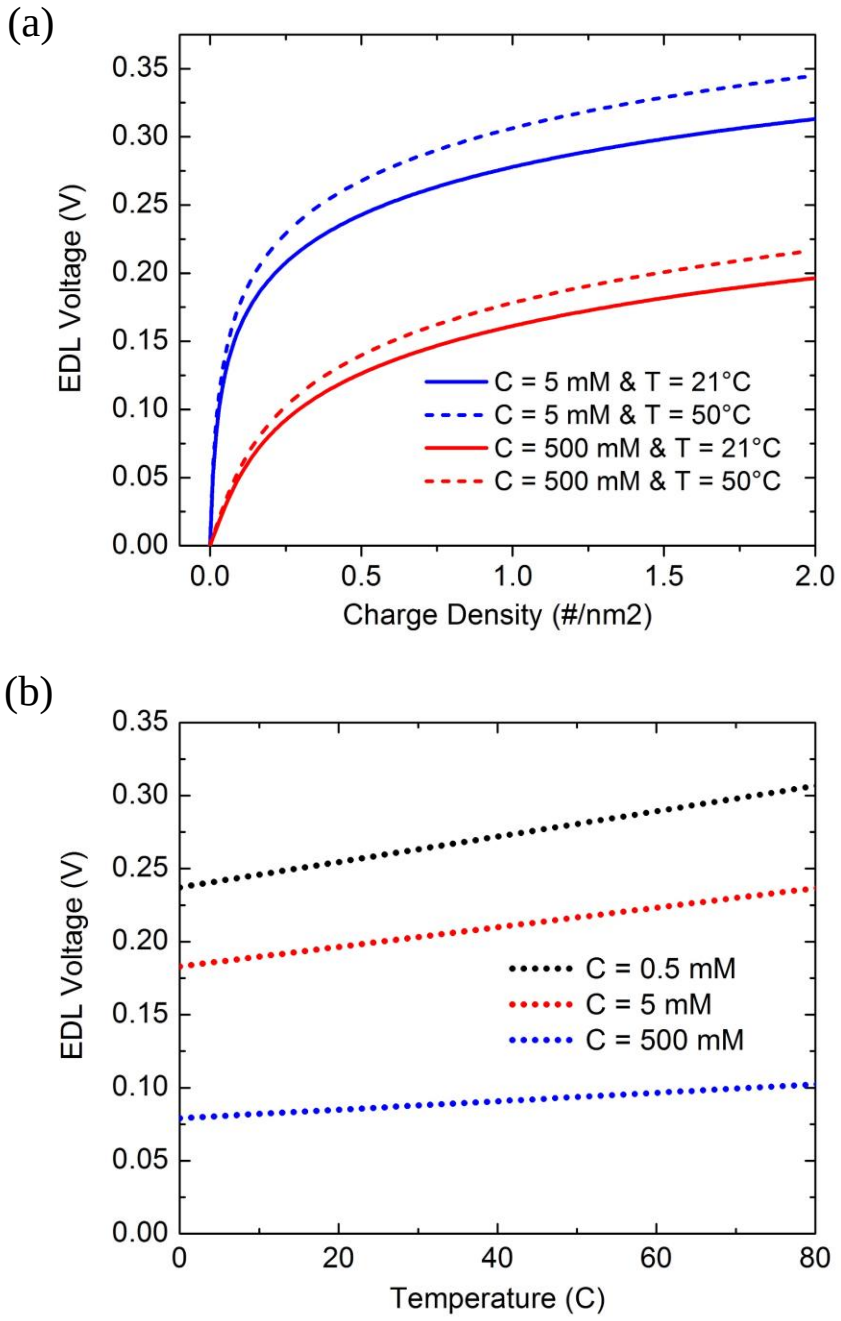

Figure 17: Theoretical computation of EDL voltage based on Gouy-Chapman-Stern (GCS) model and Poisson-Boltzmann equation at experimental operating conditions. (a) Temperature dependence of EDL voltages for 3 different salt concentration. (b) The change of EDL voltage with respect to the charge density for different operational conditions

Based on GCS model for EDL theory, a Stern layer near the electrode surface is considered for the effect of ion size, so the double layer voltage is the sum of Stern layer voltage V_d and diffuse layer voltage V_{st}, which equals to half of cell voltage. By assuming the stern layer capacity C_{st} as a constant value (2 F/m^2), the surface charge density σ can be derived from Equation 8-11 in section 2.5.3 [101]. The change of σ with increasing cell voltages is theoretically explored at different salt concentration (Figure 18a).

To theoretically characterize the charge efficiency of CDI, salt ions per unit of electrode surface area is firstly evaluated from the EDL voltage profile. A Cartesian coordinate is established to position in the double layer structure, where x denotes the distance from the electrode surface plane, and y is the non-dimensional double layer voltage. The integral of salt concentration gradient over the diffuse layer volume provides the ion adsorption density Γ_{salt}, which is shown in Equation 10.

$$\Gamma_{salt} = 2c_s \int_0^{\infty} (\cosh y - 1) dx = \frac{8c_s}{\kappa} \sinh^2(\frac{V_d}{4V_T}) \tag{17}$$

where c_s is salt concentration, κ is inverse of Debye length, and V_T is the thermal voltage. From the surface charge density σ and ion adsorption density Γ_{salt}, the charge efficiency is derived shown in Equation 18.

$$\Lambda = \frac{\Gamma_{salt}}{\sigma} = \tanh(\frac{V_d}{4V_T}) \tag{18}$$

Theoretical charge efficiency is numerically solved (Appendix A2) and is further plotted versus the cell voltage as using different salt concentrations and Stern layer capacities (Figure 18b). The theoretically obtained results indicates that greater charge efficiency is achieved at higher Stern capacitance and lower ionic strength. As increasing cell voltage from 0 to 1 volts, the charge efficiency approaches to unity but without intersection, which is confirmed by the effect of co-ion exclusion.

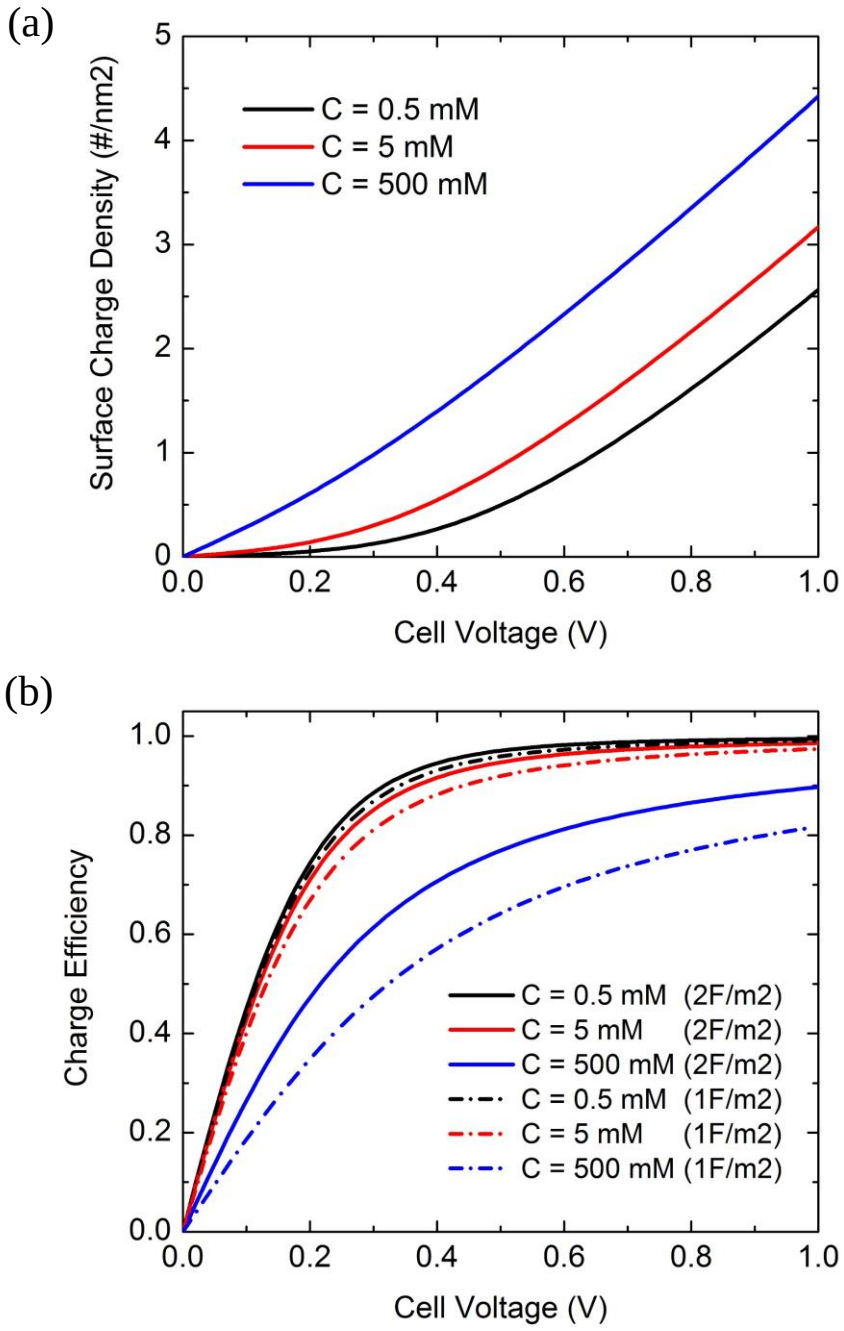

Figure 18: (a) The electrical surface charge density versus cell voltage at different salt concentration. The corresponding theoretical method is based on GCS model. (b) The charge efficiency at different salt concentration and Stern layer capacity is plotted with respect to the cell voltage.

4.2 Effect of Temperature

The temperature effect on electrochemical features and desalination performances of CDI and MCDI cell are explored in this section. CV technique is utilized to determine the gravimetric specific capacitance of porous carbon electrodes at 3 different temperature (21°C, 35°C and 50°C). The salt concentrations of NaCl solution flowing through the cells are 5 mM and 500 mM, and different potential sweep rates are applied to generate CV diagrams (Figure 19). Based on the experimental data, the specific capacitance is calculated using Equation 14. As using 2 mV/s sweep rate and 500 mM salt concentration, the specific capacitances are 112.85, 114.97 and 116.47 F/g at temperature of 21°C, 35°C and 50°C. For the same salt concentration but using higher sweep rate (10 mV/s), the specific capacitance increases from 48.80 F/g to 61.11 F/g as rising temperature from 21°C to 50°C (~25.2% improvement). Same trend is observed at salt concentration of 5 mM, where the porous electrodes shows around 22.5% higher capacitance at 50°C compared to the room temperature.

EIS technique is applied to generate the Nyquist diagrams of CDI or MCDI cells, which reveals the resistive and capacitive elements of solid-electrolyte interface. The Nyquist diagrams of MCDI cell is generated as using 5 mM or 500 mM NaCl solution at three operating conditions (Figure 20a and b). The shape of a semicircle followed by an inclined tail reveals the electrochemical features of the internal system (see section 3.3.2). Specifically, the starting and the end point of the semicircle indicates the internal resistance R_s and charge transfer resistance R_{CT}, and the radius is positively related to the double

layer capacitance C_{DL}. The temperature influence on those elements can be qualitatively described based on the Nyquist diagrams. For both salt concentration used in the experiments, warmer operational condition leads to smaller cell internal resistance and higher double layer capacitance. This trend implies that higher temperature is beneficial for a reduced IR loss while discharging the cell and an improved ion storage capacity. Furthermore, the quantitative values of the capacitive and resistance elements are obtained by simulating the experimental data with an equivalent electrical circuits, which is shown in Table 1. As increasing temperature from 21°C to 50°C with 5 mM NaCl solution used, the internal resistance decreased around 17.8% while the double layer capacitance increased about 25.8%.

(a)

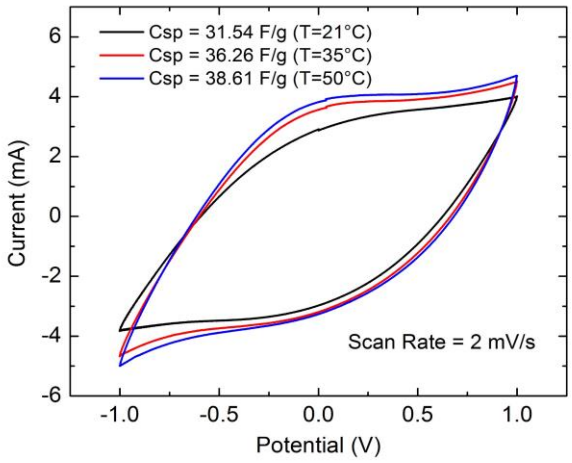

(b)

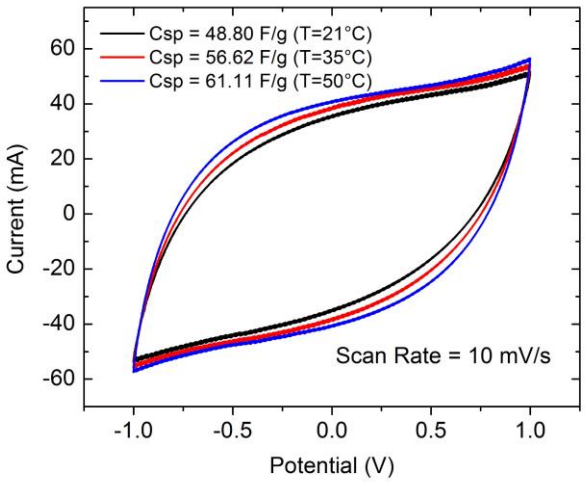

(c)

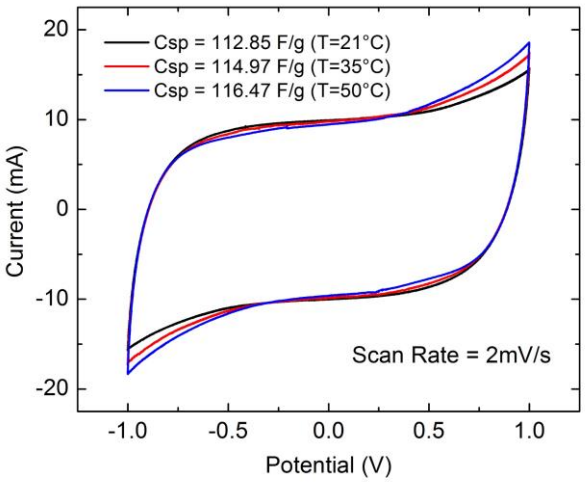

Figure 19: The cyclic voltammetry (CV) diagrams of CDI cell at different temperatures (21°C, 35°C, 50°C). (a) The potential sweep rate is 2 mV/s and salt concentration is 5 mM. (b) The potential sweep rate is 10 mV/s and salt concentration is 500 mM. (c) The potential sweep rate is 2 mV/s and salt concentration is 500 mM.

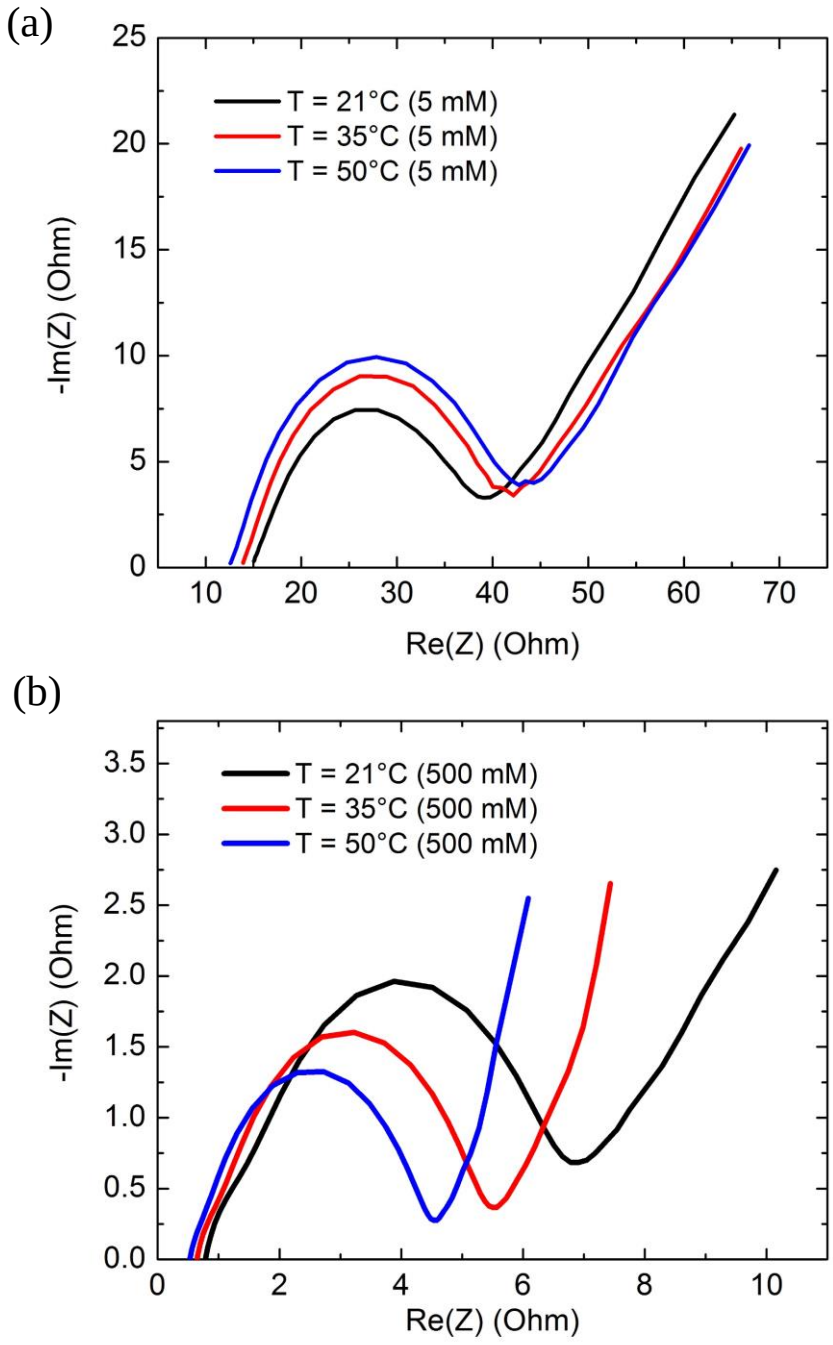

Figure 20: The Nyquist diagrams of MCDI cell at different temperature (21°C, 35°C, 50°C) obtained from EIS technique. (a) The salt concentration of NaCl solution is 5 mM. (b) The salt concentration of NaCl solution is 500 mM.

Moreover, the temperature effect on salt removal capability of CDI and MCDI cell is investigated by operating the traditional charging-discharge cycles under constant voltage method. During the experiments, the current response and conductivity values are recorded to determine various desalination parameters. The continuous cycles are controlled as an isothermal process, which means the temperature of ion adsorption and desorption steps is constant. The CDI or MCDI cell is tested both at room temperature and 35°C, while other operational conditions are kept the same.

Figure 21 shows the fluctuations in salt concentration as charging and discharging the MCDI cell at 1.2 V and -1.2V for 1 hour of each step. In this operating condition, increasing temperature enables the cell to remove more salt ions. The salt removal percentage at 21°C and 35°C are 34.84±0.24 and 38.94±0.38. The SAC values at 35°C is calculated as 9.71±0.04 mg/g, which is around 10% higher than that at room temperature (8.83±0.07 mg/g). The input and output electrical charge in coulomb is computed by the integral over the time of one step. Based on the amount of salt adsorption and electric charge transferred, the charge efficiencies at 21°C and 35°C are calculated as 0.67±0.04 and 0.77±0.03 (15% more at higher temperature). The enhancement in salt removal in MCDI cell is possibly due to the higher double layer voltage and capacitance at higher temperature, which is demonstrated in CV and EIS studies. This trend observed in experiments also agrees with the theoretical modellings.

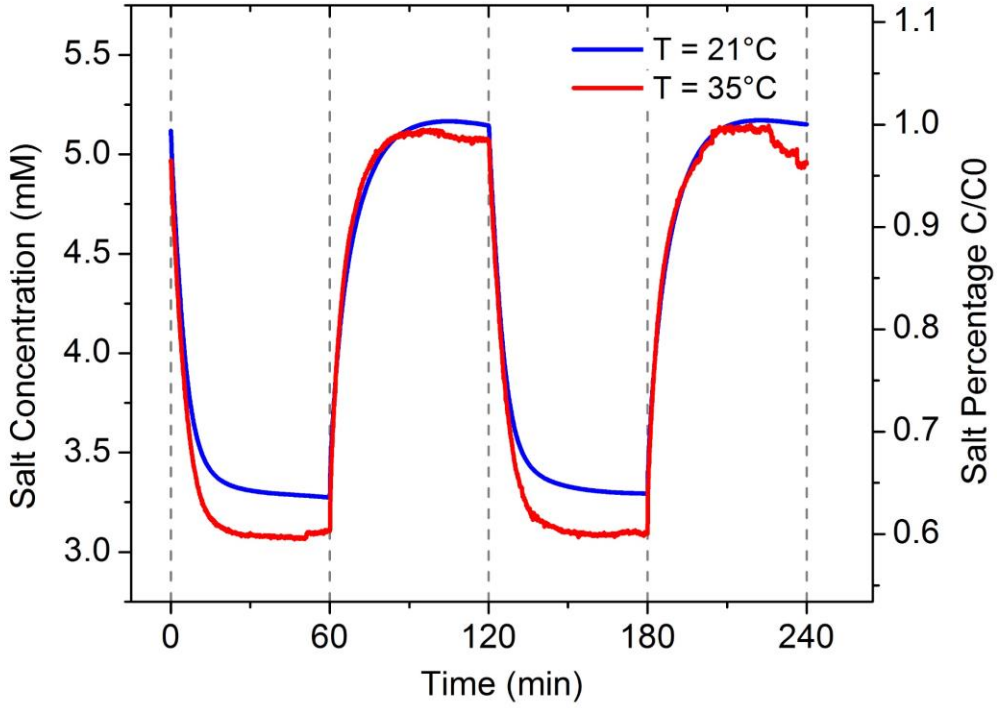

Figure 21: The temperature effect on the salt removal of MCDI. The cell is charged and discharged at 1.2 V and -1.2 V for 1 hour at each step, and is operated isothermally at two temperature (21°C and 35°C).

The salt removal for both CDI and MCDI cell at two operating temperatures are evaluated as applying various charging voltages in multiple cycles. The experimental procedures are described in section 3.3. The current and conductivity values in each cycle are used to calculate standard system parameters with performing statistical analysis. The coulombic efficiency that defined as the ratio between input and output charge, and SAC are calculated for CDI and MCDI cells (Figure 22a and b).

For MCDI cell, the coulombic efficiency and SAC increase with temperature in almost all cases. The coulombic efficiency remains a relatively stable level at room temperature as varying the charging voltages, but at 35°C, it reaches highest values (0.86±0.03) at 1.2V. While the salt adsorption capacity has a positive relationship with the applied voltage, since higher charging voltages increases the electric surface charge density, allowing for more ion adsorption in EDL. However, none or even negative influence of rising temperature on salt removal is observed at high voltage.

For CDI cell, the experimental results exhibit an opposite trend of the temperature effect compared to MCDI, which is seen that lower coulombic efficiency and SAC are obtained at higher temperature. The degraded salt removal performance may have following reasons. On one hand, increasing temperature promotes the kinetic energy and thermal motion of salt ions, which counteracts with the ion immobilization in EDL. On the other hand, temperature rising intensities the co-ion exclusion effects, which boost the co-ions leaves the porous electrode without hindrance of ion exchange membranes.

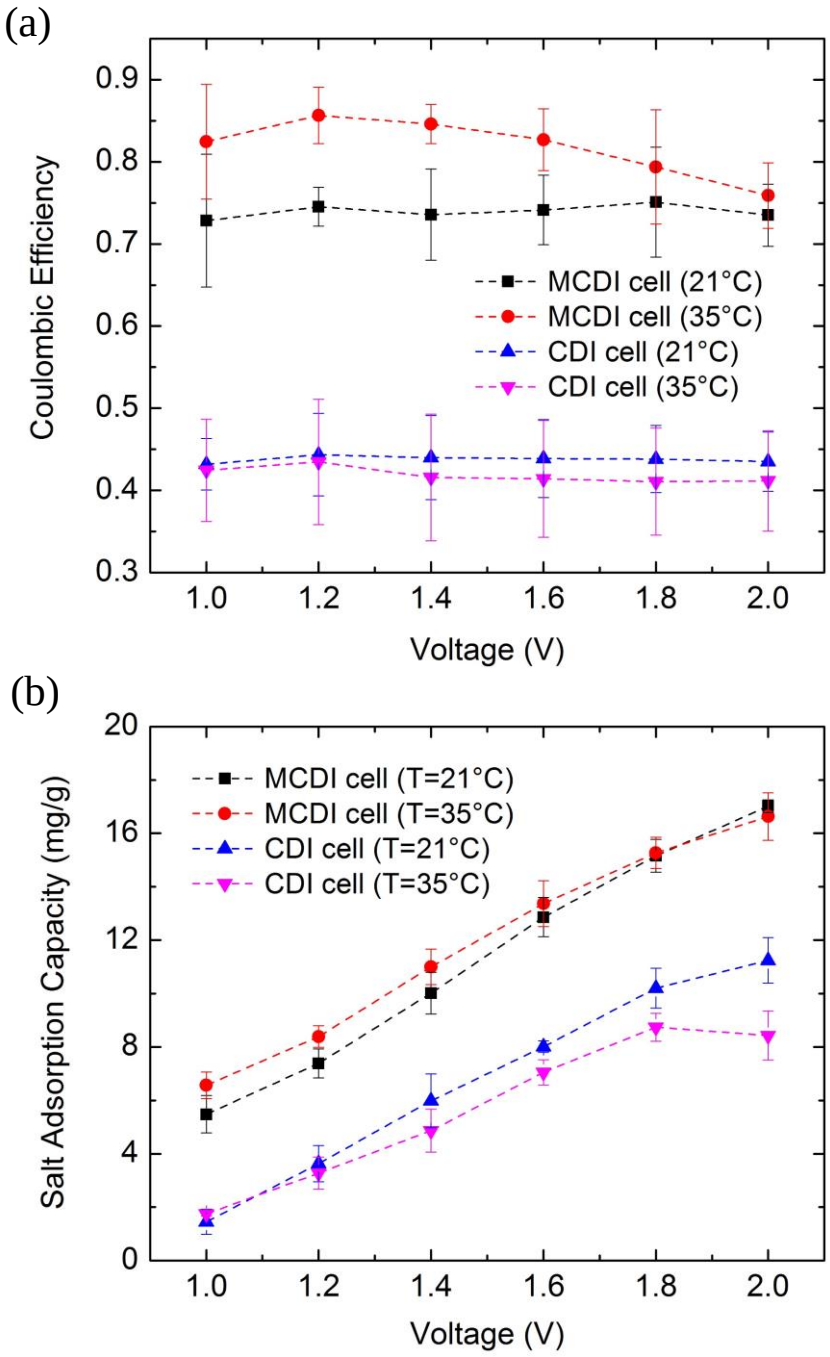

Figure 22: Temperature effect on CDI and MCDI cell at various charging voltages. (a) The change of the coulombic efficiency with applied voltage at 21°C and 35°C. (b) The change in salt adsorption capacity with applied voltage at 21°C and 35°C.

4.3 Effect of Salt Concentration

The salt concentration of feed water in CDI or MCDI strongly affects the electrochemical features of the cell. Theoretical analysis in section 4.1 demonstrates that EDL potential, surface charge density and charge efficiency are all dependent on salt concentration. Experimentally, the salinity effect on the MCDI cell is mainly discovered by EIS technique. Three sample NaCl solution with different ion concentrations (0.5 mM, 5 mM and 500 mM) subsequently flows through the cell, while EIS is performed in a frequency range from 200 kHz to 10 mHz. From Nyquist diagrams, the resistive and capacitive elements of electrode-electrolyte interface were explored at different salinities (Figure 23). When using diluted NaCl solution (0.5 mM), extremely high internal resistance R_s and charge transfer resistance R_{CT} is observed, due to small volumetric density of charge carrier in the electrolyte. In the meantime, lower salinity yields higher double layer capacitance C_{DL}, which is consistent with the theoretical predictions [101]. The general trend indicates that R_s, R_{CT} and C_{DL} all decreases as increasing the salt concentration of NaCl solution.

The precise values of the capacitive and resistive elements are shown in Table 1. For the sample NaCl solution used in desalination tests (5 mM), the internal resistance and charge transfer resistance of MCDI cell are 19.63±0.39 Ω and 20.65±1.40 Ω. As switching to 0.5 mM salt solution, R_s increases 6.7 times, and R_{CT} increases 3.0 times. While 0.5 M NaCl is used, R_s and R_{CT} decreases 25.5 and 3.2 times respectively.

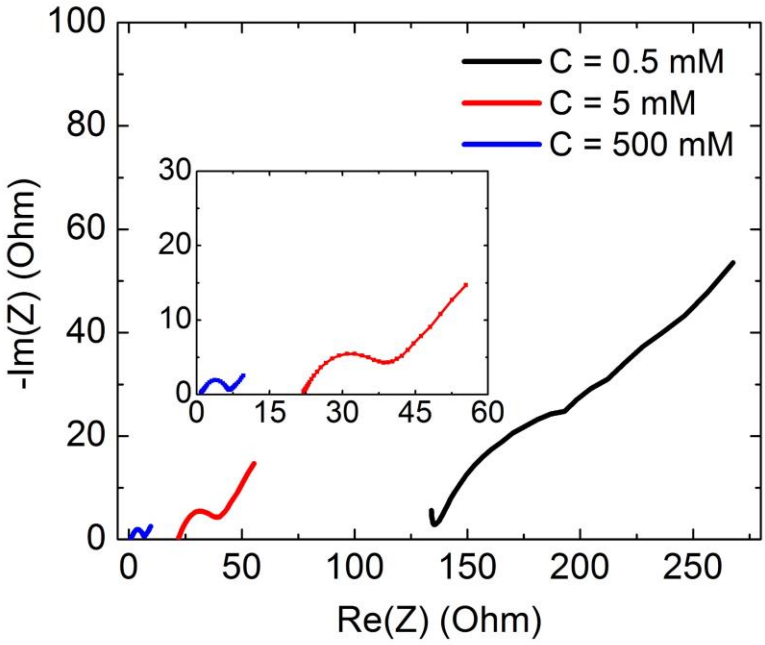

Figure 23: Nyquist diagram of MCDI cell generated by EIS technique. Three NaCl solution (0.5 mM, 5 mM and 500 mM) is used at room temperature to investigate the effect of salt concentration.

Table 1: Quantitative values of resistive and capacitive elements of the MCDI cell. An equivalent electrical circuit is used to simulate the Nyquist diagrams generated by EIS technique. The MCDI cell is operated at 3 different salt concentrations and temperatures.

	R_s (Ω)	C_{DL} (μF)	R_{CT} (Ω)	W ($\Omega . s^{-0.5}$)
5 mM (21°C)	19.63 ± 0.39	73.47 ± 3.31	20.65 ± 1.40	12.40 ± 0.68
5 mM (35°C)	17.64 ± 0.38	88.03 ± 3.42	19.97 ± 1.35	11.65 ± 0.70
5 mM (50°C)	16.14 ± 0.38	92.39 ± 4.51	19.01 ± 1.43	10.68 ± 0.69
500 mM (21°C)	0.77 ± 0.11	36.08 ± 1.54	6.36 ± 0.31	2.46 ± 0.23
500 mM (35°C)	0.65 ± 0.16	41.68 ± 2.16	4.83 ± 0.25	1.30 ± 0.22
500 mM (50°C)	0.53 ± 0.14	46.73 ± 2.95	3.88 ± 0.30	1.13 ± 0.20
0.5 mM (21°C)	131.90 ± 2.69	114.00 ± 4.84	61.09 ± 4.68	46.63 ± 1.65

4.4 Energy Analysis

This section presents the effects of salt concentration and temperature of on the energy recovery in MCDI as applying constant current method. Traditional operating mode uses same salinities of brackish water for both desalination and electrode regeneration processes, and runs consistently at room temperature. In a 3-stroke cycle (Charging-OCV-discharge) we applied in experiments, the carbon electrodes are open-circuit flushed and discharged by different salinities of brine, and also at different temperatures. The impacts of varying salt concentration and temperature are individually interpreted based on several factors, which all affects the total energy consumption throughout the cycle.

To explore the impact of recycling brine stream on energy recovery, the MCDI cell is charged at 3 mA to desalinate 25 mL NaCl solution (c=5 mM) in all experiments. Once the cell voltage reaches 2 V, an OCV mode follows to flush the carbon electrode with 0.5 mM, 5 mM, and 500 mM salt solutions for different cycles (Figure 24a). The cell voltage in OCV region was amplified for explanations in details (Figure 24b). The initial change in voltage at different salt concentration was interpreted by EDL theory. The electron charges build up on the electrode surface to attract counter-ions during the charging phase. Through this process, EDL forms at the interface between the electrode and the salt solution. From the theoretical modeling in section 4.1, higher EDL voltage is obtained at lower salt concentration. Thus, highest voltage is measured for 0.5 mM ionic concentration at the beginning of OCV, and then the cell voltage gradually drops for all different salt solution due to the effect of electron charge leakage.

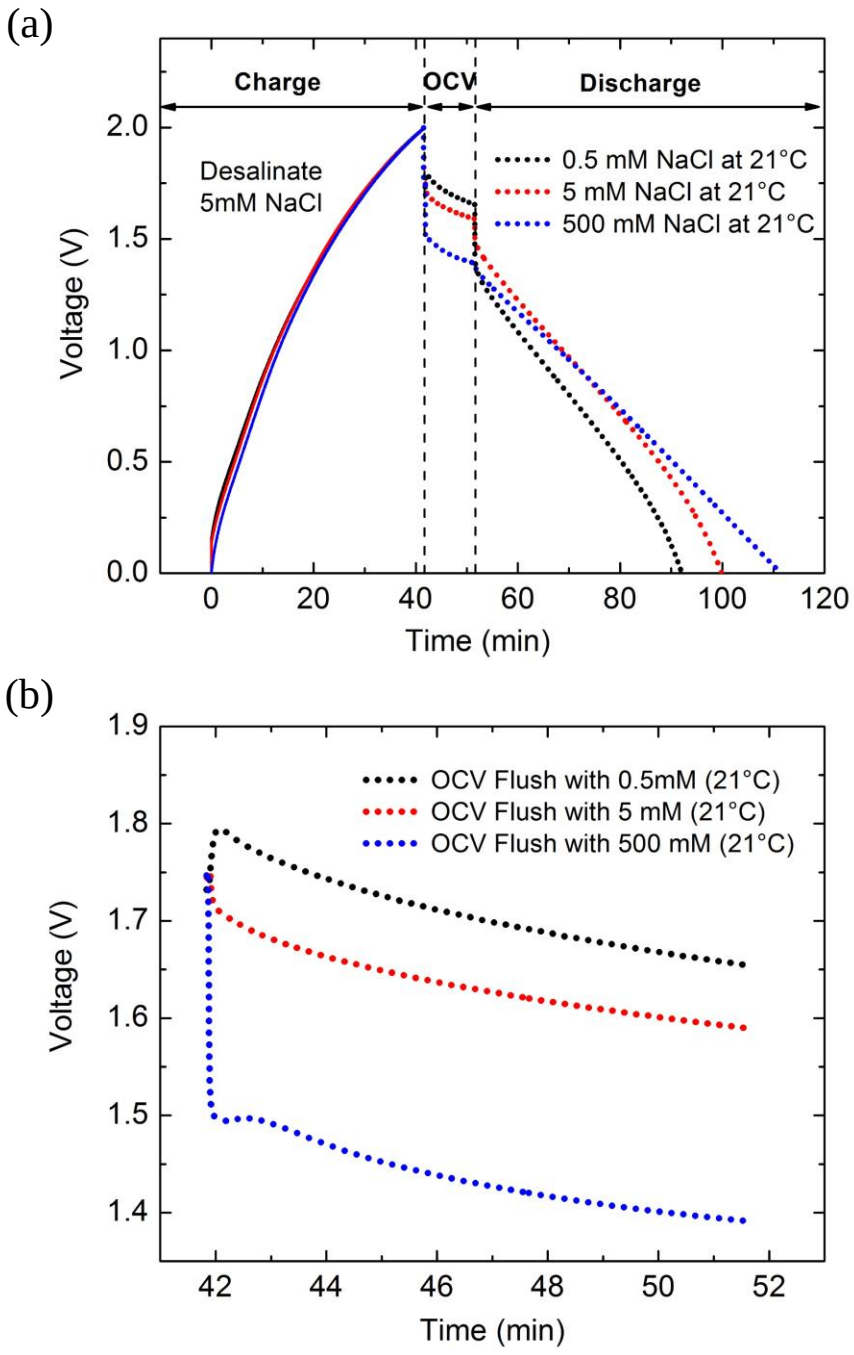

Figure 24: (a) 3-stroke MCDI cycle including constant current (3mA) charging with 5mM NaCl, open-circuit (OCV) flush, and reverse-current discharge with different brine concentration. (b) Voltage drop for different concentration of salt water during OCV step.

At the moment that MCDI cell switches to the discharge step, another jump in voltage appears, which is caused by the overpotential (IR drop). It is proportional to the Ohmic resistance that mainly related to the electrolyte, and also includes the impedance from electrodes and membranes. Note that the salt solution used for discharging the electrodes is the same as the one in OCV step. Based on EIS technique (see section 3.3.2), the resistive and capacitive elements of MCDI cell are obtained by simulating the Nyquist diagrams with an equivalent electrical circuit. The Ohmic resistance R_s of highest salinity (c=500 mM) is approximately 25 times lower than that of 5 mM, and 170 times lower than that of 0.5 mM salt concentration at room temperature. As a result, the concentrated brine solution significantly reduces the overpotential, which shows negligible voltage drop at the beginning of discharge step, In contrast, the dilute stream (c=0.5 mM) with high Ohmic resistance cause much greater IR drop. Furthermore, the slope of discharge curve correlates to Ohmic resistance R_s and charge transfer resistance R_{CT}. From section 4.3, the magnitude of both two resistive elements are extremely small when the highly concentrated brine is used. The discharge voltage, accordingly, decrease in a smaller rate compared with the other two salinities, which is consistent with the discharge slopes measured in experiments.

The electrical energy required to overcome the resistive elements in MCDI cell cannot be recovered. This implies that high salinity of brine can reduce the energy loss due to the low Ohmic resistance. Although lower EDL voltage at high concentration induces additional drop in cell voltage, the reduction in cell resistance can compensate this negative effect, and even potentially gains more recoverable energy during the discharge phase. The cell voltages measured throughout the cycle are plotted with respect to surface charge

density, and the enclosed area represents the net electrical work (Figure 25). As increasing the salt concentration of solution (c=0.5 mM, 5 mM, and 500 mM) used for flushing and discharging the electrodes, the total energy consumption per unit of desalinated water is calculated as 229.45±4.66 kJ/m^3, 208.71±2.93 kJ/m^3, and 191.23±3.60 kJ/m^3. In practice, recycling the brine stream used for regenerating carbon electrodes can achieve higher water recovery ratio. The salt concentration of such brine stream increases at the same time, which contribute to more recoverable energy.

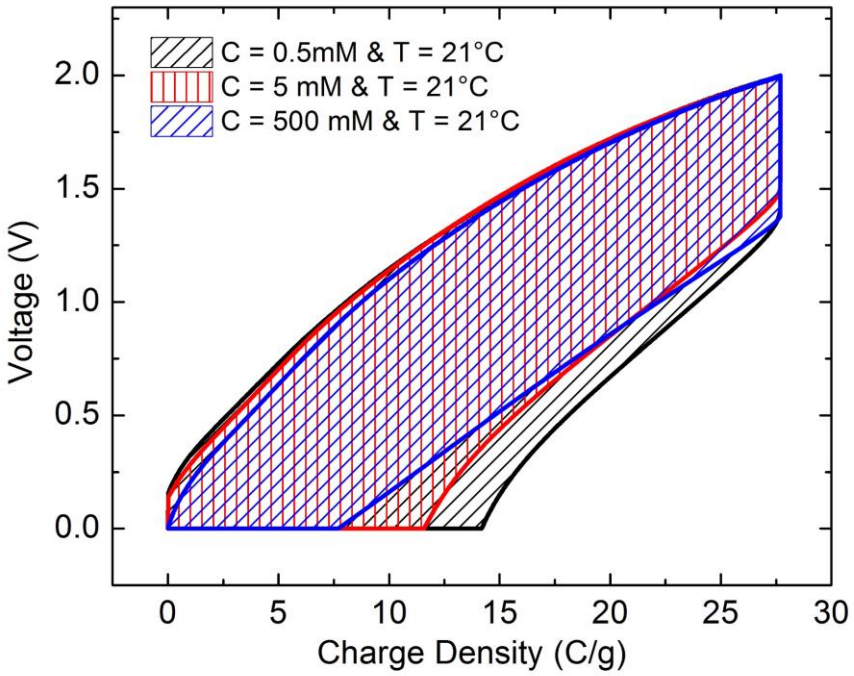

Figure 25: The net electric work represented as the integral of the cell voltage over the surface charge density. At three different salinities (0.5 mM, 5 mM and 500 mM) of the NaCl solution used for open-circuit flushing and discharging the electrode, the overall energy consumptions are calculated as 229.45±4.66 kJ/m^3, 208.71±2.93 kJ/m^3, and 191.23±3.60 kJ/m^3 respectively.

Similarly, the effect of increasing temperature on energy recovery is investigated within a 3-stroke cycle (Figure 26a). For all the testing cycles, 5mM NaCl solution (T=21°C) is fed into the MCDI cell, where constant current of 3mA is applied during the charging step. The area under the charging voltage curve is proportional to the electrical energy invested for ion adsorption. Since the operational conditions are kept the same during the charging step, the input energy is approximately matching. At the moment that OCV flushing starts, the flow electrolyte was switched to 500 mM concentrated brine at various temperature (T = 21°C, 35°C and 50°C) in different 3-stroke cycles. Based on the theoretical modeling in section 4.1, the EDL voltage is positively correlated with temperature while keeping the salt concentration and surface charge density at constant. Increasing temperature leads to a thermal voltage rise of EDL, so the highest level of cell voltage is measured as flowing the brine stream at 50°C in OCV region (Figure 26b). After stepping into the discharge phase, the cycle operated at higher temperature shows greater initial voltage, which has potential to recover more energy. The temperature effect on MCDI cell resistance is described in section 4.2, where Figure 14b shows the Nyquist diagrams of MCDI cell at 3 temperatures as using the concentrated brine stream (c=500 mM). The resistance elements R_s and R_{CT} in the equivalent circuit both decrease as rising the temperature (Table 1). However, the brine concentrated with salt ions has extremely low resistance, making the temperature effect negligible.

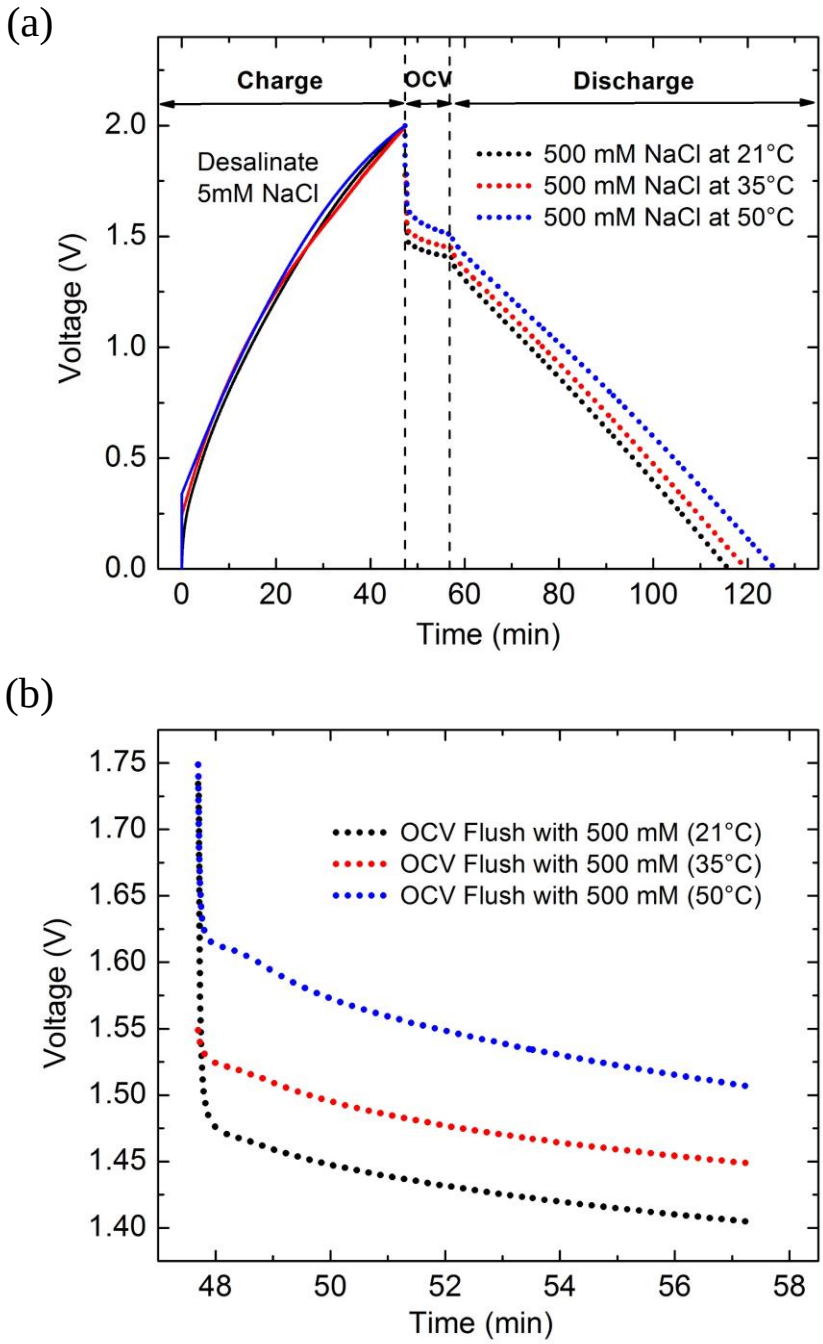

Figure 26: (a) 3-stroke MCDI cycle operated using constant-current mode: the cell was charged at 3mA for desalting 5mM NaCl solution, followed by OCV flush and reverse-current discharge with 500 mM brine at different temperatures (21°C, 35°C, 50°C). (b) Voltage drop during OCV at different temperatures.

The integral of cell voltage over the surface charge density reveals the net electrical work under 3 different conditions, shown in Figure 21. The specific energy consumptions at 21°C, 35°C and 50°C are computed as 191.23±3.60 kJ/m^3, 185.41±2.45 kJ/m^3, and 176.55±1.71 kJ/m^3 respectively. This implies that providing thermal energy to the MCDI cell is beneficial for recovering additional electrical energy. The energy recovery ratio is calculated through dividing the energy recovered during the discharge step by the electrical energy consumed for charging the cell. Table 2 lists the values of consumed electrical energy, recoverable electrical energy, net electrical work and energy recovery ratio under different operational conditions (temperature and salinities). Compared to the traditional operating mode (c=5 mM, T=21°C), flushing and discharging the MCDI cell by 500 mM concentrated brine improves the energy recovery from 33.85% to 37.50%. Increasing the temperature of brine stream to 50°C further boost the value to 42%. Therefore, the optimum conditions used in this study can potentially reduce more than 15% of overall electrical energy consumption throughout the 3-stroke cycle.

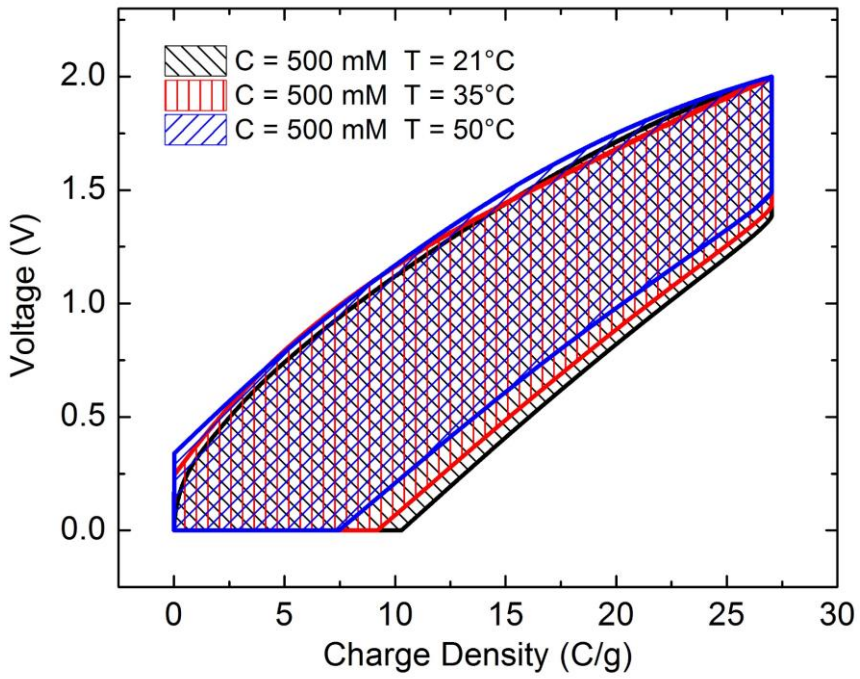

Figure 27: The overall energy consumption in 3-stroke cycles where the effect of temperature on energy recovery is investigated. 500 mM concentrated brine is used to open-circuit flush and discharge the electrode at three different temperature (21°C, 35°C and 35°C), and the overall energy consumption are calculated as 191.23±3.60 kJ/m^3, 185.41±2.45 kJ/m^3, and 176.55±1.71 kJ/m^3.

Table 2: The energy analysis under different operating conditions (temperature and salinity) in 3-stroke intermittent cycle (Charging-OCV-Discharge).

	Consumed Electrical Energy (kJ/m^3)	Recoverable Electrical Energy (kJ/m^3)	Net Electrical Energy (kJ/m^3)	Energy Recovery Ratio (%)
0.5 mM (21°C)	318.94 ± 3.97	89.49 ± 1.77	229.45 ± 4.66	28.06
5 mM (21°C)	315.51 ± 2.59	106.80 ± 1.40	208.71 ± 2.94	33.85
500 mM (21°C)	305.96 ± 3.31	114.73 ± 2.28	191.23 ± 3.60	37.50
500 mM (35°C)	304.28 ± 2.35	118.87 ± 0.80	185.41 ± 2.45	39.07
500 mM (50°C)	304.60 ± 2.55	128.06 ± 1.26	176.55 ± 1.71	42.04

CONCLUSIONS

Capacitive Deionization (CDI) is a promising alternative to state-of-the-art technologies for desalinating brackish water due to low energy consumption and economic cost. CDI removes salt ions from feed water through an electrosorption process induced by an electrical voltage difference. Discharging the electrodes to regenerate its adsorption capacity can partially recover the electrical energy, however, this become difficult as the brine (waste solution) becomes concentrated. In order to maintain high energy recovery during high water recovery testing (~80-95%), new desalination cycles need to be employed.

Here, a heat-combined MCDI system is investigated for higher energy efficiency and salt removal processes. The energy analysis in a 3-stroke operational cycle reveals that higher salinity and temperature of brine used for discharging the electrodes contributes to greater energy and water recovery. Under this condition, experimental results indicate that the net electrical work reduce more than 15% compared to the traditional operating mode. Furthermore, increasing the operational temperature to a small extent is able to improve the MCDI salt adsorption capacity nearly 10%.

Potential future work should addressed on the theoretical explanations of heat addition into the CDI separation cycles from a ‘carnot’ efficiency limit. An exergy analysis along with EDL theories can also aid in demonstrating the theoretical efficiency of waste

heat utilization in desalination cycles. The thermal effects on MCDI overall energy consumption should also evaluated under constant voltage mode, to mimic direct current systems. The limits on the potential operating temperature during the charging or discharge step, and the change in electrical energy consumed and recovered can be analyzed in future studies.

APPENDIX A. MATLAB code

A.1 MATLAB for EDL potential

```
%%%%%%%%%%%%%%%%%%%%%%%%%%%%%%%%%%%%%%%%%%%%%%%%%%%%%%%%%%%%%%%%%%%%%%%%%%%%
%  FILENAME:                    EDL Theoretical Modeling
%  WRITTEN BY:                  Jiankai Zhang
%                               Georgia Institute of Technology
%
%  COMMENTS ON CODE STRUCTURE:  This code theoretically calculates the
%                               Electric Double layer at different salt
%                               concentration and temperature
%
%  ORIGINAL DATA WRITTEN:       03 April 2016 - Water Lab.
%
%%%%%%%%%%%%%%%%% START OF JIANKAI ZHANG's CODE
%%%%%%%%%%%%%%%%%%%%%%%%%%%


clear all;
clc;

%Define charge density range
Cd = (0:0.01:2);

%Fundamental Constant for Modified Poisson-Boltzmann Equation

kb = 1.38065e-23; %Posisson-Boltzmann Constant(1.38e-23 J/K = 8.617e-5
eV/K)
e = 1.602176e-19; %Elementary Charge
Na = 6.02214e23;  %Avogadro's constant (Na = 6.022e23 mole-1)
E0 = 8.8542e-12;  %Electric constant (Eo = 8.8542e-12 F/m)


%Define Variables

T1 = 294.15;      %Temperature (25°C)
T2 = 323.15;      %Temperature (45°C)
Rs1 = 5e-3;       %Salt Concentration in molar
Rs2 = 0.5;        %Salt Concentration in molar

%Calculate the dielectric constant

Er1=(87.88-0.39*(T1-273.15)+0.00072*(T1-273.15).^2)*(1.0-
0.2551*Rs1+0.05151*Rs1^2-0.006889*Rs1^3);
Er2=(87.88-0.39*(T2-273.15)+0.00072*(T2-273.15).^2)*(1.0-
0.2551*Rs1+0.05151*Rs1^2-0.006889*Rs1^3);
Er3=(87.88-0.39*(T1-273.15)+0.00072*(T1-273.15).^2)*(1.0-
0.2551*Rs2+0.05151*Rs2^2-0.006889*Rs2^3);
Er4=(87.88-0.39*(T2-273.15)+0.00072*(T2-273.15).^2)*(1.0-
0.2551*Rs2+0.05151*Rs2^2-0.006889*Rs2^3);
```

```
%Calculate EDL potential

v1 = ((2*kb*T1)/e).*(asinh(Cd/(sqrt(8*1000*Rs1*Na*E0*Er1*kb*T1'))));
v2 = ((2*kb*T2)/e).*(asinh(Cd/(sqrt(8*1000*Rs1*Na*E0*Er2*kb*T2'))));
v3 = ((2*kb*T1)/e).*(asinh(Cd/(sqrt(8*1000*Rs2*Na*E0*Er1*kb*T1'))));
v4 = ((2*kb*T2)/e).*(asinh(Cd/(sqrt(8*1000*Rs2*Na*E0*Er2*kb*T2'))));

%Make the plot of EDL potential versus temperature
plot(Cd,v1,'-b',Cd,v2,'-.b',Cd,v3,'-r',Cd,v4,'-.r')
title('Double Layer voltage vs. Charge density')
xlabel('Charge density (#/nm^2)')
ylabel('Electrode Potential(V)')
legend('C= 5mM, T=21°C','C= 5mM, T=50°C','C= 0.5M, T=21°C','C= 0.5M,
T=50°C')
```

A.2 MATLAB for Charge Efficiency

```
%%%%%%%%%%%%%%%%%%%%%%%%%%%%%%%%%%%%%%%%%%%%%%%%%%%%%%%%%%%%%%%%%%%%%%%%%%%%
%  FILENAME:                    Charge Efficiency Modeling
%  WRITTEN BY:                  Jiankai Zhang
%                               Georgia Institute of Technology
%
%  COMMENTS ON CODE STRUCTURE:  This code calculates the charge
effciency
%                               as afunction of cell voltage, stern
capacity
%                               and ionic strength
%
%  ORIGINAL DATA WRITTEN:       27 Feburary 2016 - Water Lab.
%
%%%%%%%%%%%%%%%%% START OF JIANKAI ZHANG's CODE
%%%%%%%%%%%%%%%%%%%%%%%%%%%

clear all;
clc;

%% Parameter setup

Vc = (0:0.01:1);      % Total cell voltage
Cbm1 = 0.0005;        % Bulk inoinc concentration in molar
Cbm2 = 0.005;         % Bulk inoinc concentration in molar
Cbm3 = 0.5;           % Bulk inoinc concentration in molar
bl = 0.72e-9;         % Bjerrum length at room temperature
e = 1.602176e-19;     % Elementary Charge
Cst1 = 2;             % Stern layer capacity
Cst2 = 1;             % Stern layer capacity
Vt = 0.0256;          % Thermal voltage of water at room temperature
R = 8.314;            % Universal gas constant
T = 298;              % Room temperature
Na = 6.022e23;        % Avogradro constant

% Calculate inverse of the Debye length at different ionic strength

kappa1 = sqrt(8*pi*bl*Cbm1*Na*1000);
kappa2 = sqrt(8*pi*bl*Cbm2*Na*1000);
kappa3 = sqrt(8*pi*bl*Cbm3*Na*1000);



%% Case 1: Stern layer capacitance = 2F/m^2; Bult concentration = 10 mM

v1 = 4*(Cbm1*Na*1000*e)/(Cst1*kappa1);

for i = 1:101;
    syms x
    m = Vc(i);
    f = x -(v1*sinh(0.5/Vt*(0.5*m-x)));
```

```
    Vst1(i) = feval(symengine, 'numeric::solve', f==0, x,
'AllRealRoots');

end

Vst1 = double(Vst1);          % Stern Layer Voltage

Vd1 = Vc-2*Vst1;              % Diffuse Layer Voltage

Sc1 = (Cst1*Vst1./e)*10e-19; % Surface Charge density

Ceff1 = tanh (Vd1./0.2);      % Charge effciency


%% Case 2: Stern layer capacitance = 2F/m^2; Bult concentration = 1 mM

v2 = 4*(Cbm2*Na*1000*e)/(Cst1*kappa2);

for i = 1:101;
    syms x
    m = Vc(i);
    f = x -(v2*sinh(0.5/Vt*(0.5*m-x)));
    Vst2(i) = feval(symengine, 'numeric::solve', f==0, x,
'AllRealRoots');

end

Vst2 = double(Vst2);          % Stern Layer Voltage

Vd2 = Vc-2*Vst2;              % Diffuse Layer Voltage

Sc2 = (Cst1*Vst2./e)*10e-19; % Surface Charge density

Ceff2 = tanh (Vd2./0.2);      % Charge effciency



%% Case 3: Stern layer capacitance = 2F/m^2; Bult concentration = 100
mM

v3 = 4*(Cbm3*Na*1000*e)/(Cst1*kappa3);

for i = 1:101;
    syms x
    m = Vc(i);
    f = x -(v3*sinh(0.5/Vt*(0.5*m-x)));
    Vst3(i) = feval(symengine, 'numeric::solve', f==0, x,
'AllRealRoots');

end

Vst3 = double(Vst3);          % Stern Layer Voltage
```

```
Vd3 = Vc-2*Vst3;              % Diffuse Layer Voltage

Sc3 = (Cst1*Vst3./e)*10e-19; % Surface Charge density

Ceff3 = tanh (Vd3./0.2);      % Charge effciency


%% Case 4: Stern layer capacitance = 1F/m^2; Bult concentration = 10 mM

v4 = 4*(Cbm1*Na*1000*e)/(Cst2*kappa1);

for i = 1:101;
    syms x
    m = Vc(i);
    f = x -(v4*sinh(0.5/Vt*(0.5*m-x)));
    Vst4(i) = feval(symengine, 'numeric::solve', f==0, x,
'AllRealRoots');

end

Vst4 = double(Vst4);          % Stern Layer Voltage

Vd4 = Vc-2*Vst4;              % Diffuse Layer Voltage

Sc4 = (Cst2*Vst4./e)*10e-19; % Surface Charge density

Ceff4 = tanh (Vd4./0.2);      % Charge effciency




%% Case 5: Stern layer capacitance = 1F/m^2; Bult concentration = 1 mM

v5 = 4*(Cbm2*Na*1000*e)/(Cst2*kappa2);

for i = 1:101;
    syms x
    m = Vc(i);
    f = x -(v5*sinh(0.5/Vt*(0.5*m-x)));
    Vst5(i) = feval(symengine, 'numeric::solve', f==0, x,
'AllRealRoots');

end

Vst5 = double(Vst5);          % Stern Layer Voltage

Vd5 = Vc-2*Vst5;              % Diffuse Layer Voltage

Sc5 = (Cst2*Vst5./e)*10e-19; % Surface Charge density

Ceff5 = tanh (Vd5./0.2);      % Charge effciency
```

```
%% Case 6: Stern layer capacitance = 1F/m^2; Bult concentration = 100
mM

v6 = 4*(Cbm3*Na*1000*e)/(Cst2*kappa3);

for i = 1:101;
    syms x
    m = Vc(i);
    f = x -(v6*sinh(0.5/Vt*(0.5*m-x)));
    Vst6(i) = feval(symengine, 'numeric::solve', f==0, x,
'AllRealRoots');

end

Vst6 = double(Vst6);          % Stern Layer Voltage

Vd6 = Vc-2*Vst6;              % Diffuse Layer Voltage

Sc6 = (Cst2*Vst6./e)*10e-19; % Surface Charge density

Ceff6 = tanh (Vd6./0.2);      % Charge effciency


%% Plot the surface charge density and charge efficiency

% Plot the surface charge density for different stern layer capacity

 h1 = figure(1);
 set(h1,'Name','Surface charge density for different stern layer
capacity');
 plot(Vc,Sc1,Vc,Sc4)
 title ('Surface charge density vs cell voltage (C=10mM)')
 xlabel('Cell Voltage(V)')
 ylabel('Suface Charge (#/nm^2)')
 legend('Stern layer capacity = 2F/m^2','Stern layer capacity =
1F/m^2')

 % Plot the surface charge density for different ionic strength

 h2 = figure(2);
 set(h2,'Name','Surface charge density for different bulk ionic
strength');
 plot(Vc,Sc1,Vc,Sc2,Vc,Sc3)
 title ('Surface charge density vs cell voltage (Cst=2F/m^2))')
 xlabel('Cell Voltage(V)')
 ylabel('Suface Charge (#/nm^2)')
 legend('C=1mM','C=10mM','C=100mM')

 % Plot the charge effiency vs Cell voltage

 h3 = figure(3);
```

```
set(h3,'Name','GCS model charge efficiency');
plot(Vc,Ceff1,'-b',Vc,Ceff2,'-r',Vc,Ceff3,'-k',Vc,Ceff4,'-
.b',Vc,Ceff5,'-.r',Vc,Ceff6,'-.k')
title ('Charge efficiency Analysis for GCS model')
xlabel('Cell Voltage(V)')
ylabel('Charge efficiency')
legend('C=1mM Cst=2F/m^2','C=10mM Cst=2F/m^2','C=100mM Cst=2F/m^2',...
    'C=1mM Cst=1F/m^2','C=10mM Cst=1F/m^2','C=100mM Cst=1F/m^2')
```

REFERENCES

[1] Porada S, Zhao R, Van Der Wal A, Presser V, Biesheuvel P. Review on the science and technology of water desalination by capacitive deionization. Progress in Materials Science. 2013;58:1388-442.

[2] Suss M, Porada S, Sun X, Biesheuvel P, Yoon J, Presser V. Water desalination via capacitive deionization: what is it and what can we expect from it? Energy & Environmental Science. 2015;8:2296-319.

[3] Karagiannis IC, Soldatos PG. Water desalination cost literature: review and assessment. Desalination. 2008;223:448-56.

[4] Rijsberman FR. Water scarcity: fact or fiction? Agricultural water management. 2006;80:5-22.

[5] Abu-Zeid MA. Water and sustainable development: the vision for world water, life and the environment. Water policy. 1998;1:9-19.

[6] Ng KC, Thu K, Kim Y, Chakraborty A, Amy G. Adsorption desalination: an emerging low-cost thermal desalination method. Desalination. 2013;308:161-79.

[7] Shiklomanov IA. Appraisal and assessment of world water resources. Water international. 2000;25:11-32.

[8] Lattemann S, Kennedy MD, Schippers JC, Amy G. Global desalination situation. Sustainability Science and Engineering. 2010;2:7-39.

[9] Greenlee LF, Lawler DF, Freeman BD, Marrot B, Moulin P. Reverse osmosis desalination: water sources, technology, and today's challenges. Water research. 2009;43:2317-48.

[10] Cipollina A, Micale G, Rizzuti L. Seawater desalination: conventional and renewable energy processes: Springer Science & Business Media; 2009.

[11] Fritzmann C, Löwenberg J, Wintgens T, Melin T. State-of-the-art of reverse osmosis desalination. Desalination. 2007;216:1-76.

[12] Zhao R. Theory and operation of capacitive deionization systems2013.

[13] El-Dessouky HT, Ettouney HM, Al-Roumi Y. Multi-stage flash desalination: present and future outlook. Chemical Engineering Journal. 1999;73:173-90.

[14] Anderson MA, Cudero AL, Palma J. Capacitive deionization as an electrochemical means of saving energy and delivering clean water. Comparison to present desalination practices: Will it compete? Electrochimica Acta. 2010;55:3845-56.

[15] Porada S, Weinstein L, Dash R, Van Der Wal A, Bryjak M, Gogotsi Y, et al. Water desalination using capacitive deionization with microporous carbon electrodes. ACS applied materials & interfaces. 2012;4:1194-9.

[16] Zou L, Morris G, Qi D. Using activated carbon electrode in electrosorptive deionisation of brackish water. Desalination. 2008;225:329-40.

[17] Nadakatti S, Tendulkar M, Kadam M. Use of mesoporous conductive carbon black to enhance performance of activated carbon electrodes in capacitive deionization technology. Desalination. 2011;268:182-8.

[18] Huang Z-H, Wang M, Wang L, Kang F. Relation between the charge efficiency of activated carbon fiber and its desalination performance. Langmuir. 2012;28:5079-84.

[19] Seo S-J, Jeon H, Lee JK, Kim G-Y, Park D, Nojima H, et al. Investigation on removal of hardness ions by capacitive deionization (CDI) for water softening applications. Water Research. 2010;44:2267-75.

[20] Sharma K, Mayes RT, Kiggans Jr J, Yiacoumi S, Gabitto J, DePaoli DW, et al. Influence of temperature on the electrosorption of ions from aqueous solutions using mesoporous carbon materials. Separation and Purification Technology. 2013;116:206-13.

[21] El-Deen AG, Barakat NA, Khalil KA, Motlak M, Kim HY. Graphene/SnO 2 nanocomposite as an effective electrode material for saline water desalination using capacitive deionization. Ceramics International. 2014;40:14627-34.

[22] Han L, Karthikeyan K, Anderson MA, Gregory KB. Exploring the impact of pore size distribution on the performance of carbon electrodes for capacitive deionization. Journal of colloid and interface science. 2014;430:93-9.

[23] Kim T, Dykstra J, Porada S, Van Der Wal A, Yoon J, Biesheuvel P. Enhanced charge efficiency and reduced energy use in capacitive deionization by increasing the discharge voltage. Journal of colloid and interface science. 2015;446:317-26.

[24] Park K-H, Kwak D-H. Electrosorption and electrochemical properties of activated-carbon sheet electrode for capacitive deionization. Journal of Electroanalytical Chemistry. 2014;732:66-73.

[25] Lee J-H, Bae W-S, Choi J-H. Electrode reactions and adsorption/desorption performance related to the applied potential in a capacitive deionization process. Desalination. 2010;258:159-63.

[26] Porada S, Bryjak M, Van Der Wal A, Biesheuvel P. Effect of electrode thickness variation on operation of capacitive deionization. Electrochimica Acta. 2012;75:148-56.

[27] Yang J, Zou L, Song H, Hao Z. Development of novel MnO 2/nanoporous carbon composite electrodes in capacitive deionization technology. Desalination. 2011;276:199-206.

[28] Zhao R, Biesheuvel P, Miedema H, Bruning H, Van der Wal A. Charge efficiency: a functional tool to probe the double-layer structure inside of porous electrodes and application in the modeling of capacitive deionization. The Journal of Physical Chemistry Letters. 2009;1:205-10.

[29] Welgemoed T, Schutte C. Capacitive deionization technology™: an alternative desalination solution. Desalination. 2005;183:327-40.

[30] Oren Y. Capacitive deionization (CDI) for desalination and water treatment—past, present and future (a review). Desalination. 2008;228:10-29.

[31] Wang G, Pan C, Wang L, Dong Q, Yu C, Zhao Z, et al. Activated carbon nanofiber webs made by electrospinning for capacitive deionization. Electrochimica Acta. 2012;69:65-70.

[32] Biesheuvel P, Zhao R, Porada S, Van der Wal A. Theory of membrane capacitive deionization including the effect of the electrode pore space. Journal of Colloid and Interface Science. 2011;360:239-48.

[33] Lee J-Y, Seo S-J, Yun S-H, Moon S-H. Preparation of ion exchanger layered electrodes for advanced membrane capacitive deionization (MCDI). Water research. 2011;45:5375-80.

[34] Biesheuvel P, Van der Wal A. Membrane capacitive deionization. Journal of Membrane Science. 2010;346:256-62.

[35] Li H, Zou L. Ion-exchange membrane capacitive deionization: a new strategy for brackish water desalination. Desalination. 2011;275:62-6.

[36] Kim Y-J, Choi J-H. Improvement of desalination efficiency in capacitive deionization using a carbon electrode coated with an ion-exchange polymer. Water research. 2010;44:990-6.

[37] Długołęcki P, van der Wal A. Energy recovery in membrane capacitive deionization. Environmental science & technology. 2013;47:4904-10.

[38] Zhao R, Porada S, Biesheuvel P, Van der Wal A. Energy consumption in membrane capacitive deionization for different water recoveries and flow rates, and comparison with reverse osmosis. Desalination. 2013;330:35-41.

[39] Zhao R, Biesheuvel P, Van der Wal A. Energy consumption and constant current operation in membrane capacitive deionization. Energy & Environmental Science. 2012;5:9520-7.

[40] Li H, Gao Y, Pan L, Zhang Y, Chen Y, Sun Z. Electrosorptive desalination by carbon nanotubes and nanofibres electrodes and ion-exchange membranes. Water Research. 2008;42:4923-8.

[41] Kang J, Kim T, Shin H, Lee J, Ha J-I, Yoon J. Direct energy recovery system for membrane capacitive deionization. Desalination. 2016;398:144-50.

[42] Kim Y-J, Hur J, Bae W, Choi J-H. Desalination of brackish water containing oil compound by capacitive deionization process. Desalination. 2010;253:119-23.

[43] Lee J-B, Park K-K, Eum H-M, Lee C-W. Desalination of a thermal power plant wastewater by membrane capacitive deionization. Desalination. 2006;196:125-34.

[44] Jeon S-i, Yeo J-g, Yang S, Choi J, Kim DK. Ion storage and energy recovery of a flow-electrode capacitive deionization process. Journal of Materials Chemistry A. 2014;2:6378-83.

[45] Jeon S-i, Park H-r, Yeo J-g, Yang S, Cho CH, Han MH, et al. Desalination via a new membrane capacitive deionization process utilizing flow-electrodes. Energy & Environmental Science. 2013;6:1471-5.

[46] Hatzell KB, Iwama E, Ferris A, Daffos B, Urita K, Tzedakis T, et al. Capacitive deionization concept based on suspension electrodes without ion exchange membranes. Electrochemistry Communications. 2014;43:18-21.

[47] García-Quismondo E, Santos C, Lado J, Palma Js, Anderson MA. Optimizing the energy efficiency of capacitive deionization reactors working under real-world conditions. Environmental science & technology. 2013;47:11866-72.

[48] Han L, Karthikeyan K, Gregory KB. Energy Consumption and Recovery in Capacitive Deionization Using Nanoporous Activated Carbon Electrodes. Journal of The Electrochemical Society. 2015;162:E282-E8.

[49] BLAIR JW, MURPHY GW. Electrochemical demineralization of water with porous electrodes of large surface area. ACS Publications; 1960.

[50] Evans S, Accomazzo M, Accomazzo J. Electrochemically Controlled Ion Exchange I. Mechanism. Journal of the Electrochemical Society. 1969;116:307-9.

[51] Murphy G, Caudle D. Mathematical theory of electrochemical demineralization in flowing systems. Electrochimica Acta. 1967;12:1655-64.

[52] Johnson AM, VENOLIA W. The electrosorb process for desalting water. 1970.

[53] Johnson A, Newman J. Desalting by means of porous carbon electrodes. Journal of the Electrochemical Society. 1971;118:510-7.

[54] Soffer A, Folman M. The electrical double layer of high surface porous carbon electrode. Journal of Electroanalytical Chemistry and Interfacial Electrochemistry. 1972;38:25-43.

[55] Oren Y, Soffer A. Water desalting by means of electrochemical parametric pumping. Journal of Applied Electrochemistry. 1983;13:473-87.

[56] Oren Y, Soffer A. Electrochemical parametric pumping. Journal of the Electrochemical Society. 1978;125:869-75.

[57] Murphy GW, Bloomfield J, Smith F, Neptune W, Purdue J. Demineralization of saline water by electrically-induced adsorption on porous carbon electrodes. Available from the National Technical Information Service, Springfield VA 22161 as PB-181 589, Price codes: A 05 in paper copy, A 01 in microfiche OSW Research and Development Progress Report. 1964.

[58] Murphy GW. Activated carbon used as electrodes in electrochemical demineralization of saline water. 1969.

[59] Rouquerol J, Avnir D, Fairbridge C, Everett D, Haynes J, Pernicone N, et al. Recommendations for the characterization of porous solids (Technical Report). Pure and Applied Chemistry. 1994;66:1739-58.

[60] Biesheuvel P, Van Limpt B, Van der Wal A. Dynamic adsorption/desorption process model for capacitive deionization. The journal of physical chemistry C. 2009;113:5636-40.

[61] Biesheuvel P, Bazant M. Nonlinear dynamics of capacitive charging and desalination by porous electrodes. Physical review E. 2010;81:031502.

[62] Cohen I, Avraham E, Noked M, Soffer A, Aurbach D. Enhanced charge efficiency in capacitive deionization achieved by surface-treated electrodes and by means of a third electrode. The Journal of Physical Chemistry C. 2011;115:19856-63.

[63] Oh H-J, Lee J-H, Ahn H-J, Jeong Y, Kim Y-J, Chi C-S. Nanoporous activated carbon cloth for capacitive deionization of aqueous solution. Thin Solid Films. 2006;515:220-5.

[64] Farmer JC, Fix DV, Mack GV, Pekala RW, Poco JF. The use of capacitive deionization with carbon aerogel electrodes to remove inorganic contaminants from water. Low level waste conference, Orlando1995.

[65] Farmer JC, Fix DV, Mack GV, Pekala RW, Poco JF. Capacitive deionization of NaCl and NaNO3 solutions with carbon aerogel electrodes. Journal of the Electrochemical Society. 1996;143:159-69.

[66] Farmer JC, Bahowick SM, Harrar JE, Fix DV, Martinelli RE, Vu AK, et al. Electrosorption of chromium ions on carbon aerogel electrodes as a means of remediating ground water. Energy & fuels. 1997;11:337-47.

[67] Gabelich CJ, Tran TD, Suffet IM. Electrosorption of inorganic salts from aqueous solution using carbon aerogels. Environmental science & technology. 2002;36:3010-9.

[68] Yang C-M, Choi W-H, Na B-K, Cho BW, Cho WI. Capacitive deionization of NaCl solution with carbon aerogel-silicagel composite electrodes. Desalination. 2005;174:125-33.

[69] Zhai Y, Dou Y, Zhao D, Fulvio PF, Mayes RT, Dai S. Carbon materials for chemical capacitive energy storage. Advanced materials. 2011;23:4828-50.

[70] Li L, Zou L, Song H, Morris G. Ordered mesoporous carbons synthesized by a modified sol–gel process for electrosorptive removal of sodium chloride. Carbon. 2009;47:775-81.

[71] Wen X, Zhang D, Shi L, Yan T, Wang H, Zhang J. Three-dimensional hierarchical porous carbon with a bimodal pore arrangement for capacitive deionization. Journal of Materials Chemistry. 2012;22:23835-44.

[72] Porada S, Borchardt L, Oschatz M, Bryjak M, Atchison J, Keesman K, et al. Direct prediction of the desalination performance of porous carbon electrodes for capacitive deionization. Energy & Environmental Science. 2013;6:3700-12.

[73] Gabelich CJ, Xu P, Cohen Y. Concentrate treatment for inland desalting. Sustainability Science and Engineering. 2010;2:295-326.

[74] Ajayan PM, Zhou OZ. Applications of carbon nanotubes. Carbon nanotubes: Springer; 2001. p. 391-425.

[75] Zhang D, Shi L, Fang J, Dai K, Li X. Preparation and desalination performance of multiwall carbon nanotubes. Materials Chemistry and Physics. 2006;97:415-9.

[76] Zou L. Developing nano-structured carbon electrodes for capacitive brackish water desalination: INTECH Open Access Publisher; 2011.

[77] Yan C, Zou L, Short R. Single-walled carbon nanotubes and polyaniline composites for capacitive deionization. Desalination. 2012;290:125-9.

[78] Nie C, Pan L, Liu Y, Li H, Chen T, Lu T, et al. Electrophoretic deposition of carbon nanotubes–polyacrylic acid composite film electrode for capacitive deionization. Electrochimica Acta. 2012;66:106-9.

[79] Stoller MD, Ruoff RS. Best practice methods for determining an electrode material's performance for ultracapacitors. Energy & Environmental Science. 2010;3:1294-301.

[80] Tsouris C, Mayes R, Kiggans J, Sharma K, Yiacoumi S, DePaoli D, et al. Mesoporous carbon for capacitive deionization of saline water. Environmental science & technology. 2011;45:10243-9.

[81] Biesheuvel P, Porada S, Levi M, Bazant M. Attractive forces in microporous carbon electrodes for capacitive deionization. Journal of solid state electrochemistry. 2014;18:1365-76.

[82] Xu P, Drewes JE, Heil D, Wang G. Treatment of brackish produced water using carbon aerogel-based capacitive deionization technology. Water research. 2008;42:2605-17.

[83] Suss ME, Baumann TF, Bourcier WL, Spadaccini CM, Rose KA, Santiago JG, et al. Capacitive desalination with flow-through electrodes. Energy & Environmental Science. 2012;5:9511-9.

[84] Zhao R, Satpradit O, Rijnaarts H, Biesheuvel P, Van der Wal A. Optimization of salt adsorption rate in membrane capacitive deionization. Water research. 2013;47:1941-52.

[85] Suss ME, Baumann TF, Worsley MA, Rose KA, Jaramillo TF, Stadermann M, et al. Impedance-based study of capacitive porous carbon electrodes with hierarchical and bimodal porosity. Journal of Power Sources. 2013;241:266-73.

[86] Kondrat S, Wu P, Qiao R, Kornyshev AA. Accelerating charging dynamics in subnanometre pores. Nature materials. 2014;13:387-93.

[87] Kim T, Yoo HD, Oh SM, Yoon J. Potential sweep method to evaluate rate capability in capacitive deionization. Electrochimica Acta. 2014;139:374-80.

[88] Kim T, Yoon J. CDI ragone plot as a functional tool to evaluate desalination performance in capacitive deionization. RSC Advances. 2015;5:1456-61.

[89] Veerman J, Saakes M, Metz SJ, Harmsen G. Reverse electrodialysis: evaluation of suitable electrode systems. Journal of Applied Electrochemistry. 2010;40:1461-74.

[90] Avraham E, Noked M, Bouhadana Y, Soffer A, Aurbach D. Limitations of charge efficiency in capacitive deionization II. On the behavior of CDI cells comprising two activated carbon electrodes. Journal of the Electrochemical Society. 2009;156:P157-P62.

[91] Avraham E, Bouhadana Y, Soffer A, Aurbach D. Limitation of charge efficiency in capacitive deionization I. On the behavior of single activated carbon. Journal of the Electrochemical Society. 2009;156:P95-P9.

[92] Porada S, Weingarth D, Hamelers H, Bryjak M, Presser V, Biesheuvel P. Carbon flow electrodes for continuous operation of capacitive deionization and capacitive mixing energy generation. Journal of Materials Chemistry A. 2014;2:9313-21.

[93] Bourcier WL, Aines RD, Haslam JJ, Schaldach CM, O'brien KC, Cussler E. Deionization and desalination using electrostatic ion pumping. Google Patents; 2011.

[94] Porada S, Sales B, Hamelers H, Biesheuvel P. Water desalination with wires. The journal of physical chemistry letters. 2012;3:1613-8.

[95] Kornyshev AA. Double-layer in ionic liquids: paradigm change? : ACS Publications; 2007.

[96] Helmholtz Hv. Ueber einige Gesetze der Vertheilung elektrischer Ströme in körperlichen Leitern mit Anwendung auf die thierisch ‐ elektrischen Versuche. Annalen der Physik. 1853;165:211-33.

[97] Bard AJ, Faulkner LR, Leddy J, Zoski CG. Electrochemical methods: fundamentals and applications: Wiley New York; 1980.

[98] Bonnefont A, Argoul F, Bazant MZ. Analysis of diffuse-layer effects on time-dependent interfacial kinetics. Journal of Electroanalytical Chemistry. 2001;500:52-61.

[99] Stojek Z. The electrical double layer and its structure. Electroanalytical methods: Springer; 2010. p. 3-9.

[100] Stern O. Zur theorie der elektrolytischen doppelschicht. Berichte der Bunsengesellschaft für physikalische Chemie. 1924;30:508-16.

[101] Biesheuvel P. Thermodynamic cycle analysis for capacitive deionization. Journal of colloid and interface science. 2009;332:258-64.

[102] Janssen M, Härtel A, Van Roij R. Boosting capacitive blue-energy and desalination devices with waste heat. Physical review letters. 2014;113:268501.

[103] Hatzell MC, Cusick RD, Logan BE. Capacitive mixing power production from salinity gradient energy enhanced through exoelectrogen-generated ionic currents. Energy & Environmental Science. 2014;7:1159-65.

[104] Masarapu C, Zeng HF, Hung KH, Wei B. Effect of temperature on the capacitance of carbon nanotube supercapacitors. ACS nano. 2009;3:2199-206.

[105] Sambriski E, Schwartz D, De Pablo J. A mesoscale model of DNA and its renaturation. Biophysical journal. 2009;96:1675-90.